

ORIGINS OF EUCRITES DEDUCED FROM
MAGMA DIFFERENTIATION MODEL

マグマ分化モデルからみたユークライト隕石の起源について

Kazuto Saiki

佐伯和人

1994

①

学位論文

Origins of eucrites deduced from magma differentiation model.

マグマ分化モデルからみたユークライト隕石の起源について

平成6年12月博士(理学)申請

東京大学大学院理学系研究科
鉱物学専攻

佐伯 和人

**Origins of eucrites deduced from
magma differentiation model.**

A Thesis
by
Kazuto Saiki

Mineralogical Institute
Graduate School of Science
University of Tokyo

Submitted for a Degree of Doctor of Science

December 22, 1994

CONTENTS

1. Introduction.	1
2. Samples and analytical methods.	8
3. Results.	10
3.1. Mineralogy and Chemistry of polymict cumulate eucrites and howardites.	10
Y791439	
Y791192	
Y82009	
Y82049	
3.2. Mineralogy and chemistry of cumulate eucrites.	21
ALH85001	
Medanitos	
Nagaria	
Y791195	
4. Computer simulations.	25
5. Discussions.	31
6. Conclusions.	40
Acknowledgments.	43
References.	44
Figures and tables.	48
Appendix I : The procedures of computer simulations.	80
Appendix II: New utilization of Differential Thermal Analyses (DTA).	99

Abstract

A group of differentiated meteorites, howardites (H), eucrites (E) and diogenites (D) have been proposed to be formed on the same parent body (HED). Cumulate eucrites have bulk chemical compositions between those of diogenites and ordinary eucrites and contain coarse-grained inverted pigeonite and homogeneous plagioclase. Mineralogy and chemistry of four polymict HED achondrites rich in cumulate eucrites; Yamato(Y)791439, Y791192, Y82009 and Y82049, and four cumulate eucrites; Medanitos, Nagaria, ALH85001 and Y791195, have been studied to gain better understanding of the origin of the HED parent body by the chemical mapping techniques developed by the author. These polymict breccias are found out to be composed of abundant cumulate eucrites and ordinary eucrites similar to Juvinas (ordinary eucrite) without other components such as remnant of primitive materials. Close association of ordinary and cumulate eucrites can be explained by a model in that they are located adjacent in the parent body crust, and that there are variety of cumulate eucrites exist at one region. To make clear the origin of cumulate eucrites, the activities of cations (Mg,Fe,Ca) in the liquid equilibrated with pyroxenes in Y791439 and some other eucrites were calculated. The results show that the liquid coexisting with cumulate eucrites is implausibly Fe-rich ($Fe\# =$ mean 70-75). Some cumulate eucrites are regarded as cumulus from evolved Fe-rich liquid, but there is no such Fe-rich clast in the HED meteorites. Compositional simulation of fractional crystallization of mafic elements with residual liquid suggest that if the cumulus includes large amount of residual trapped liquid (40-50%), a cumulate eucrite ($Fe\# =$ mean 45-50) could crystallize from ordinary eucritic liquid ($Fe\# =$ mean 60-65). For testing a "trapped-liquid model", a simulation computer program "MAGDIF" has been constructed by a method proposed by Longhi and Pan (1988) and developed by the author. The

calculated cumulate eucrite has slightly Si-poor compositions. This is an effect of crystallized olivine component. The mixture of cumulus olivine and trapped liquid has the REE pattern similar to the cumulate eucrites.

In conclusion, ordinary eucrites and many kinds of cumulate eucrite existed in almost the same region of the HED parent body and many kinds of cumulate eucrites may have existed together in a close region. Cumulate eucrites are not purely cumulus matter from evolved liquid, but they may have been produced by fractional crystallization with large amount of trapped liquid, or a mixture of fractionated crystals and residual liquid. The compositional variation among the cumulate eucrites can be reproduced by variable amounts of trapped liquid. The variation of REE patterns can also be reproduced.

1. INTRODUCTION

Historical notes on the HED achondrites

Three major classes of differentiated achondrites, howardites, eucrites and diogenites (HED meteorites), are believed to have been formed by igneous processes on the same parent body (Mason, 1962; Duke and Silver, 1967; Takeda *et al.*, 1976; Consolmagno and Drake, 1977). A candidate for such a parent body is asteroid 4 Vesta. A recent spectral study (Binzel and Chips, 1993) has confirmed a link between the HED meteorites and 4 Vesta (Gaffey, 1993).

On the basis of textures and chemistries, eucrites have been divided into a few subclasses: cumulate and non-cumulate eucrites (Mason *et al.*, 1979) or unbrecciated (crystalline), monomict, or polymict (Delaney *et al.*, 1984). A term "ordinary eucrite" has been used to designate most common type eucrite comparable to ordinary chondrites (Takeda, 1979; Nyquist *et al.*, 1986; Takeda *et al.*, 1985). They are ophitic or subophitic basalts, in which pigeonites show homogeneous chemistry of the host phases of pyroxene (pigeonite) and exhibit a fine planar exsolution texture of augite on (001). Most non-Antarctic monomict eucrites represented by Juvinas, with the exception of Pasamonte and cumulate eucrites such as Moama, Moore County, etc. are ordinary eucrites (Takeda *et al.*, 1978).

All the polymict breccias: howardites, polymict eucrites and polymict diogenites are considered to be members of a mineralogical and

compositional continuum with several lithic components mixed in varying proportions. The breccias are named after the most abundant component type. If more than 90% of a component is present, then the meteorite is named after that dominant component (Delaney et al., 1984). The polymict achondritic breccias containing more than 90% of eucritic material are polymict eucrite. The howardites are defined as polymict achondritic breccias containing less than 90% of any lithologically distinct component.

On the basis of the discovery of an intermediate lithology between diogenites and eucrites, such as Y75032, it was proposed that they are genetically related (Takeda and Mori, 1985). This hypothesis is strongly supported by the fact that the compositions of howardites are plotted on a single mixing line between eucrites and diogenites (Dreibus and Wänke, 1979).

The Y75032-type HED achondrites have been grouped on the basis of their characteristic shock textures and pyroxene compositions. Shocked pyroxene fragments slightly more Fe-rich than normal diogenites are set in dark glassy matrix. The majority of the specimens of this group (e.g., Y75032, Y791000, Y791199, and Y791422) are monomict breccias mainly of pyroxene, whose compositions fall in a limited range of Fe-rich diogenites. Y791200, Y791201, Y791073 and Y791439 are polymict breccias and contain Mg-rich cumulate eucrites in addition to Fe-rich diogenite components, and Y791439 contains rare Fe-rich ordinary eucrite clasts (Takeda, 1986; Takeda and Hidaka, 1989).

Models for origin of cumulate eucrites and ordinary eucrites

Ordinary eucrite and cumulate eucrite are usually discussed separately. This section shows how previous models treated cumulate eucrites. Many models had been proposed to explain the origin of eucrite. They are roughly separated into two groups: "Partial melting models" and "Crystal fractionation models".

The "Partial melting models" is represented by Stolper (1977) who first carried out melting experiments of natural eucrites to clarify igneous process in the formation of eucrite. The experimental results show that the bulk compositions of ordinary eucrites, which is considered to represent eucritic magma itself, are close to the olivine-pyroxene-plagioclase peritectic point of the pseudo ternary liquid system of SiO_2 -olivine-anorthite. He claimed that the melt of the peritectic point cannot be generated by fractional crystallization. He also thought that chemical equilibrium among phases during crystallization in a natural igneous process is hardly achieved. Then, he suggested that the eucritic melt is a primary magma by a partial melting of the source region which consists of olivine, pyroxene, plagioclase, chromite and metallic iron. Cumulate eucrites and diogenites as well as variation among noncumulate eucrites were explained by variation in degrees of partial melting and the following fractional crystallization processes. In this model, there is little quantitative discussion for cumulate eucrites. The location of cumulate eucrites seems to be separated from ordinary eucrites.

Bartels and Grove (1991) made further discussion for the origin of cumulate eucrites. They made melting experiments at 1bar and 1kbar and

concluded that diogenites can form by fractional crystallization from magnesian eucrite parent compositions originating as partial melts at depth within a parent body and cumulate eucrites are likely produced from such parent magmas by fractionation in plutonic environments (1kbar) with production of very iron-rich ($Mg\#=20$) residual liquids. For the origin of ordinary eucrites they accepted the Stolper's partial melt model. In their model, the compositions of cumulate eucrites has been reproduced, but the iron-rich residual liquids has not been found in our meteorite collections. The cumulate eucrites locate deep in the parent body and completely separated from ordinary eucrites.

In fractional crystallization models, the problem has been focused on how to produce eucritic melt by fractional crystallization process. The cumulate eucrites were assumed to be crystallized after the diogenite crystallization. The crystal fractionation model was revived by Ikeda and Takeda (1985) and Warren (1985), who simultaneously pointed out that the olivine pyroxene cotectic line will shift close to a line between the pyroxene and anorthite for a liquid more magnesian than the composition used by Stolper (1977) and the eucritic melt will solidify soon after the peritectic point.

Hewins and Newsom (1988) pointed out that the ol-px phase boundary in the system of SiO_2 -Ol-An can shift toward Ol side as pressure becomes high, and then it changes from a reaction to cotectic lines. They suggested a possibility that even a maximum fractionation process can generate the eucritic magma on the Ol-Px-An peritectic point by assuming a 'small' pressure drop of 1kb, rather than the equilibrium process in Stolper's model. In this model,

cumulate eucrites are not mentioned.

Longhi and Pan (1988) made a computer program on the basis of their experimental runs for simulating liquid path in fractional and equilibrium crystallization. In this program, they constructed functions of phase boundaries as function of Mg/Fe ratio and pressure from the data of their melting experiments of low-alkali basaltic materials. The results of simulation indicated that fractional crystallization at 2kbar could produce eucritic liquid. However, 2 kbar is way too high pressure for the parent body less than 250km in radius. Again in this model, there is no explanation for the origin of cumulate eucrites.

Ikeda and Takeda (1985) studied details of lithic clasts and mineral fragments in an Antarctic howardite Y7308. They proposed a model on the evolutionary process of magma ocean on the parent body, where primary magma in the ocean was produced under reducing condition by partial or batch melting of a carbonaceous or LL chondritic material. Then, fractional crystallization of the primary magma took place more or less in an open system. This fractionation process was introduced in this model to explain the continuum of chemical composition of minerals in lithic clasts and fragments. In this model, a dunite layer as the cumulates with the composition different from pallasitic olivine is produced. This model is the first model explaining all components of howardite, but many hypothetical phases are introduced. For example, trend B magma is introduced as the source of cumulate eucrites. The trend B magma must be solidified as major components in howardite, but their was found no such clast.

The problem left unsolved by all the previous models is how to produce cumulate eucrites. The easiest solution is to make cumulate eucrite at the location apart from ordinary eucrite. The presence of ordinary eucrite fragments in polymict cumulate eucrites, however, suggests ordinary eucrites were located near to cumulate eucrites. A little work has been performed to invoke the genetic link between ordinary eucrites and cumulate eucrites.

Approaches of this study

In order to gain a better understanding of the origin of cumulate eucrites and evolutionary trend of the HED parent body, the author investigated four polymict breccias Y791439, Y791192, Y82009 and Y82049 with a new chemical mapping system (Saiki et al., 1991) of the electron probe microanalysis (EPMA). For comparison with the polymict breccias, four cumulate eucrites, Medanit, Nagaria, ALH85001, and Y791195 have been observed. On the basis of these accumulated data the author defined constraints for modeling the HED parent body. In order to make the factors clear, the author calculated the activities of major elements (Fe, Mg, Ca) in equilibrium liquid coexisting with pyroxenes in the Y791439 polymict breccia and some cumulate eucrites using partition coefficient between pyroxene and liquid with modified two lattice melt model of Nielsen and Dungan (1983). He also simulated the fractional crystallization of mafic elements by originally constructed program. Mg number (mg#) ($= \text{Mg} \times 100 / (\text{Mg} + \text{Fe})$) of liquid and instantaneous solid (IS) in fractional crystallization process were calculated. IS is the solid being crystallized from the liquid at any moment. The detailed

procedure of the simulation is given in a separate section.

For satisfying the constraints, the author proposes a "trapped-liquid hypothesis". For quantitative discussion of the igneous process in the HED parent body, it is necessary to carry out computer simulation to test the phase relation and compositional changes of melt and minerals. For this purpose, a simulation program "MAGDIF" has been constructed by a method proposed by Longhi and Pan (1988) and developed by the author. It will be explained in detail in "Appendix I". In constructing this hypothetical model, a new use of Differential Thermal Analysis (DTA) experiments was performed. The details of the experiments are shown in "Appendix II".

2. SAMPLES AND ANALYTICAL METHODS

Polished thin sections (PTS's) of Y791439,51-2, Y791192,91-2, Y82009,51-2, Y82049,61-2 and Y791195,92-1 were supplied from the National Institute of Polar Research (NIPR) in Japan. Medanitos and Nagaria were supplied from the British Museum (Natural History). A PTS of ALH85001 was made from a chip supplied from the Meteorite Working Group (MWG) in the U. S.

Y791439, Y791192, and Y782009 are Y75032-type HED achondrites, Y82049 is a howardite and Y791195, Medanitos, Nagaria, and ALH85001 are cumulate eucrites.

These samples were investigated by SEM (JEOL840A) equipped with the Kevex Super 8000 EDS system, which is capable of obtaining X-ray elemental distribution map (EDX-Map). Backscattered Electron Images (BEI) and fluorescent X-ray intensity maps of up to 15 elements obtained by digital electron beam controller were converted into digital images and processed by graphics software "Kevex Advanced Imaging".

This system was connected with a personal computer (SHARP X68000) by an RS232C cable. We transferred EDX-Map intensity data from the Kevex system to the X68000 computer and processed them by the "Pyroxene Quadrilateral(PXQUAD)" system originally constructed by the author (Saiki et al., 1992). The PXQUAD system is an EDX-Map processor developed for characterizing pyroxenes of different chemistry and texture speedily. This system processes Mg-Si-Ca-Fe intensities acquired on the Kevex EDX-Map system for quantitative analysis using a modified Bence and Albee method (Nakamura and Kushiro, 1970). It calculates rough chemical compositions,

identifies pyroxene phases, and plots an elemental distribution map and the Ca-Mg-Fe trends in a pyroxene quadrilateral with the same color scale simultaneously. A color palette, showing how a particular chemical composition is assigned for each point is displayed simultaneously on the elemental distribution map image and the pyroxene quadrilateral. Ca, Fe and Mg mol% are expressed as Red, Green, and Blue% on each pixel (Fig.1). The PXQUAD software also provides us with a modal analysis tool for pyroxenes within a certain chemical range.

The chemical compositions of particular minerals on the above maps were analyzed by electron-probe microanalyser (EPMA) JEOL 733 Mark II at Geological Inst., Univ. of Tokyo, with the conditions of 15 kV accelerating voltage and 12nA sample current. The correction method for silicates and oxides was that of modified Bence and Albee method using parameters of Nakamura and Kushiro (1970). The bulk compositions of pyroxenes in Y791439 are calculated by combining the lamellae/host areal ratio obtained by the PXQUAD system and point analysis data obtained by EPMA. The bulk compositions of pyroxenes in other samples are average compositions of EPMA line analyses.

3. RESULTS

3.1. Mineralogy and Chemistry of polymict cumulate eucrites and a howardite

We studied three kinds of polymict cumulate eucrites, Y791439, Y791192 and Y82009 and one howardite, Y82049. They are polymict breccias mainly composed of cumulate eucrites with minor diogenitic and ordinary eucrite components.

We investigated an entire surface of the PTSs by the PXQUAD system and classified all pyroxenes on them. The classification is mainly based on the criteria of Delaney et al (1984). The observed variations of pyroxene are more complex than Delaney's, so the classification in this paper is slightly different from his. For example, the Binda type originally defined has only blebby augite and no lamellae, but some pyroxenes with blebby augites and thin lamellae were classified as Binda type when their chemical compositions are similar to Binda. In addition the author employed an abbreviation system for pyroxene in the following form: "pyx *number of samples in two digits* (*pyroxene type by one or two alphabets*)". For example, "pyx39(B)" stands for the Binda type pyroxene in Y791439. When there are more than one kind of pyroxene in the same Delaney-type class, sub-numbers are added. For example, pyx39(B1), pyx39(B2). Zoned pyroxenes have many variations in their compositional range. Because zoned pyroxenes are not always Pasamonte type in Delaney's classification, the author call them Z type.

Y791439

Y791439 was classified as a polymict cumulate eucrite with small diogenitic and rare ordinary eucrite components (Takeda and Hidaka, 1989). The photomicrograph of Y791439 is shown in Fig. 2a. Y791439 contains more clasts of cumulate eucrite than Y75032. Six cumulate eucrite clasts up to 2.8 x 2.3 mm with large amount of plagioclase have been found in the PTS (Takeda and Hidaka, 1989). The images of PX-QUAD system suggest that pyroxene chemical compositions of Y791439 are divided into four types; Pyx39(D), Pyx39(B), Pyx39(MC) and Pyx39(JV). The type code stand for: D:diogenitic type, B:Binda type, MC:Moore County type, and JV:Juvinas type in the decreasing order of mg number. Chemical compositions of four types of pyroxenes are shown in Fig. 3b and Table 1a. The characteristics of each pyroxene type can be described as follows:

Pyx39(D) type. The pyx39(D)-type pyroxenes are most magnesian members among the Y791439 pyroxene. The chemical compositions of this type of pyroxenes (Fig. 3a and Table 1a) are close to Binda, but because their exsolution texture is similar to diogenite, this group was classified as Diogenitic-type in Delaney's classification. Many pyroxenes have no lamella observable by SEM. In some pyx39(D) pyroxenes, thin augite lamellae less than 1 μm are detected (Fig. 5a). The lamellae are similar to typical (100) lamellae found in diogenitic clast in polymict eucrites. The PXQUAD system shows that pyroxenes with lamellae have slightly more Fe-rich compositions than those without lamella within this type.

Pyx39(B) type. The pyx39(B)-type pyroxenes are most abundant, and

many of them are preserved in their original shape within a lithic clast. The chemical compositions of the B-type pyroxenes are slightly more Fe-rich than those of Binda, but many of them have blebs (Fig. 5b) typical of Binda. The host chemical compositions of the pyx39(B)-type pyroxene are fairly uniform but their textures are somewhat variable. Some pyroxenes have thin (001) augite lamellae similar to those found in Serra de Magé (Harlow *et al.*, 1979) and their thickness are up to several microns, but are not as thick as those of Serra de Magé, and a slightly Fe- and Ca- richer composition of pyx39(B) is reported by Takeda and Hidaka (1989). This type of pyroxene must be crystallographically divided into Binda type and Moore County type on the basis of Delanys' criterion, but the author uses the term B-type for Y791439 in this paper because of their indistinguishable chemical compositions by the present method.

Pyx39(MC) type The pyx39(MC)-type pyroxenes are also brecciated severely. The chemical compositions of this pyroxene type are close to those of Moore County (Mori and Takeda, 1981). One typical pyroxene crystal 0.8 x 0.5 mm in size contains thick 20 μm (001) exsolution lamellae with 50-100 μm interval as in Moore County (Fig.5c). The structures of the host pyroxene are disturbed by shock event and show wavy extinction.

Pyx39(JV) type. The pyx39(JV)-type pyroxenes are severely brecciated to small pieces, and the original texture can not be recovered. This type pyroxene is classified as Juvinas type in Delaney's criteria. One pyroxene grain has an augite region up to 50 μm in width. This region looks like an assembly of micron sized lamellae. This unique texture will be discussed later.

Some of other pyroxenes have thin augite lamellae, several microns in width (Fig. 5d), as in Juvinas. Most of the augite is present not as lamellae but around brecciated pyroxene crystals. The chemical compositions of the pyx39(JV) pyroxenes are close to those of Juvinas, but the lamella compositions of Y791439 are more Ca poor and the host compositions of Y791439 are more Ca rich than those of Juvinas. It may be due to the incomplete resolution of the lamellae by an electron beam of EPMA.

Other minerals. The bulk chemical compositions of all four types of pyroxene (Table 1a) show a tendency for Ca and Ti concentration to increase with decreasing mg number.

The chemical compositions of plagioclase in Y791439 fall in a limited range of anorthite content (An_{90} - An_{92}) (Fig.4a). The pyx39(B)-type pyroxenes and plagioclase show an equigranular texture with rounded grain boundaries in some large clasts, but we could not correlate plagioclase type with the type of pyroxene, because most plagioclase is finely brecciated.

Y791192

Y791192 was classified as a polymict cumulate eucrite with large ordinary eucrite component and a small diagenitic component. A photomicrograph of Y791192 is shown in Fig.2b. One large ordinary eucrite clast 1.5 x 2.0 mm in size with plagioclase laths has been found in the PTS. The images of the PX-QUAD system suggest that pyroxene chemical compositions of Y791192 are divided into six types; Pyx92(D1), Pyx92(D2), Pyx92(B), Pyx92(MC1), Pyx92(MC2), and Pyx92(JV). Chemical compositions

of six types of pyroxenes are shown in Fig. 3b and Table 1b. The characteristics of each pyroxene type can be described as follows:

Pyx92(D1) type. The pyx92(D1) type pyroxenes are most magnesian members among the Y791192 pyroxene. Although this group was classified as D-type, the chemical compositions of this pyroxene type (Fig. 3b and Table 1b) are close to Binda, but there are no blebby augites as are typical in Binda. The pyroxenes of this type have no lamella observable by SEM (Fig. 6a, 6b). In one pyroxene, there is a chromite belt 1-3 μ m in width along clacks (Fig. 6b). There are Fe-rich rims less than 1 μ m wide in some pyroxenes.

Pyx92(D2) type. The pyx92(D2) type pyroxenes are the second most magnesian members among the Y791192 pyroxene. The chemical compositions of this type of pyroxenes (Fig. 3b and Table 1b) are slightly more Fe-rich than pyx92(D1) type. Thin augite lamellae less than 2 μ m are detected (Fig. 6b). The lamellae are similar to typical (100) lamellae found in diogenitic clast in polymict eucrites. A few pyroxenes have blebby augites 10 μ m in width. There are few other phases in pyroxenes, but some pyroxenes have chromites less than 10 μ m in size. There are Fe-rich rims, less than 1 μ m wide, in some pyroxenes.

Pyx92(B) type. The pyx92(B)-type pyroxene has slightly more Fe-rich chemical compositions than those of Binda (Fig. 3b, table 1b). The major exsolution texture is thin exsolution lamellae (Fig. 6b) 1-3 μ m in width, and a few pyroxenes have blebby augites (Fig. 6a). In pyx39(B), there are pyroxenes with thin exsolution lamellae. The pyx92(B) is similar to pyx39(B). There are few other phases in pyroxenes, but some pyroxenes includes chromites.

There are Fe-rich rims, less than $1\mu\text{m}$ wide, in some pyroxenes.

Pyx92(MC1) type. The pyx92(MC1)-type pyroxenes have similar chemical compositions to that of Moore County (Fig.3b, table 1b). They have thick (001) exsolution lamellae up to $30\mu\text{m}$ in width, but the texture is severely disturbed by a shock event (Fig.6a). The chromites, several microns in size, coexisting with these pyroxenes are Ti-rich.

Pyx92(MC2) type. The pyx92(MC2)-type pyroxenes have similar chemical compositions to Moore County (Fig.3b, table 1b). They are slightly more Fe-rich than pyx92(MC1)-type pyroxenes but the difference is so little, that they might be classified in the same category as pyx92(MC1). They also have thick (001) exsolution lamellae up to $20\mu\text{m}$ in width (Fig.6c). The coexisting spinels, several microns in size, have significant ulvöspinel components.

Pyx92(JV) type. The pyx92(JV)-type pyroxenes are slightly more Mg rich than Juvinas. Some pyroxenes have thin exsolution lamellae several microns in width as in Juvinas, but the pyroxenes of this type have many unique variations. The largest clast, 2.0×1.5 mm in size, contains cloudy pyroxenes (Fig.6d). The exsolution texture indicates rapid cooling history but the clouding suggests annealing at low temperature. This clast includes ilmenite. The chemical compositions of coexisting plagioclase vary in wide range (An_{77} - An_{90}). Another clast, 1.0×0.7 mm in size, has pyx92(JV)-type pyroxene with very unique texture. Pyroxenes in this clast consist of recrystallized aggregate of small Ca-rich and Ca-poor pyroxenes (Fig.6e). The chemical compositions of coexisting plagioclase is An_{64} - An_{90} . One pyroxene fragment has unique

exsolution lamellae (Fig.6f) with submicron-sized sub-lamellae both in the host and lamellae.

Other minerals. The chemical compositions of the most plagioclase in Y791192 fall in a slightly wider range of the anorthite content (An₈₃ - An₉₂). The pyx92(JV)-type pyroxenes are, however, coexisting with plagioclase of An₇₇ - An₉₀. The plagioclase fragments of the other type of pyroxenes could not be identified, because they are brecciated severely. One extremely large plagioclase fragment has chemical composition An_{91.5} - An_{92.3}. Y791192 has comparatively large amount of matrix, where one ilmenite nugget is found, 150 x 70 μ m in size (Fig.6a). It's an aggregate of small ilmenites and matrix. The nugget is mainly composed of ilmenite up to 10 μ m in size, and other part are fine grained matrix of plagioclase and pyroxene and silica minerals 10 μ m in size. Zoned Fe-rich rims are found in D1, D2, B, MC1 and MC2 type pyroxenes. They seem to have formed not by a crystallization process but by Fe/Mg diffusion from the Fe-rich matrix.

Y82009

Y82009 was classified as a polymict eucrite (Yanai and Kojima, 1987). A photomicrograph of Y82009 (Fig.2c) shows that it has a large Juvinas type clast up to 2.0 x 1.5 mm. The images of PX-QUAD system suggest that pyroxene chemical compositions of Y82009 are divided into five types; Pyx09(D), Pyx09(B), Pyx09(MC), Pyx09(JV), and Pyx09(Z) (Fig.3c and Table 1c). The characteristics of each pyroxene type can be described as follows:

Pyx09(D) type The Pyx09(D) type pyroxenes are the most magnesian members among the Y82009 pyroxene. The chemical compositions of this

type of pyroxene (Fig. 3c and Table 1c) are slightly Ca-rich than common diogenite (Mittlefehldt and Lindstrom, 1993). There is no lamella observed by SEM in this type of pyroxene. Pyroxenes of this type are zoned toward Fe-rich rims 5-6 μ m in width (Fig.7a).

Pyx09(B) type The Pyx09(B) type pyroxenes are the second most magnesian members among the Y82009 pyroxenes (Fig.7a). The chemical compositions of this type of pyroxenes (fig. 3c and table 1c) are slightly more Fe-rich than those in Binda. A few pyroxenes have small chromites less than 3 μ m in size. One pyroxene shows both lamellae texture and zoning (Fig. 7b). This remarkable texture will be discussed later.

Pyx09(MC) type. The pyx09(MC)-type pyroxenes have similar chemical compositions to other MC-type pyroxene in Y791439 and Y791192 but slightly more Ca-rich (Fig.3c and table 1c), and show no exsolution lamellae observable by SEM. A few pyroxenes include ilmenites several microns in size. This pyroxene also has a zoned rim (Fig.7c)

Pyx09(JV) type. The pyx09(JV)-type pyroxnes are rare components in Y82009. There is a possibility that Pyx09(JV) type is a part of Pyx09(Z), because the pyroxenes of this type were brecciated to small pieces (Fig.7b), and the chemical compositions of them are plotted on a part of Fe-rich zoned pyroxenes. But they have exsolution lamellae several microns in width.

Pyx09(Z) type. The pyx09(Z)-type includes all zoned pyroxenes in Y82009. Most of them are components of a large clast 2.0 x 1.6 mm in size (Fig.7d). They show chemical zoning (Fig.3c and table 1c) from mg#=18 to 64, but lamellae are not observable. The chemical composition of coexisting

plagioclase is $An_{82}-An_{87}$. The clast has mesostasis including Fe-metal, Ca-phosphates, Ca-rich pyroxene and abundant ilmenite.

There are many variations in ranges of the chemical composition, but it is very difficult to classify their zoning trends. Some pyroxene has Fe-rich pyroxene vein along clacks (Fig.7e). Some plagioclases paired with this type of pyroxene show chemical compositions $An_{83}-An_{93}$.

Other minerals. The chemical compositions of plagioclase in Y82009 fall in a wide range of anorthite content ($An_{75} - An_{94}$). The author could not identify pairing of plagioclase with the pyroxenes of a particular type, because they are fragmented severely into small grains. The plagioclase in the large clast with the Pyx09(Z)-type pyroxene has chemical compositions of $An_{82}-An_{87}$. Most plagioclases paired with this type of pyroxene are $An_{83}-An_{93}$. The plagioclases with lower anorthite contents than An_{82} are small pieces and their paired pyroxenes could not be found.

Y82049

Y82049 was classified as a polymict eucrite (Yanai and Kojima, 1987). The photomicrograph of the Y82049 PTS (Fig. 2d) shows that two large clasts 1.1 x 2.0 mm and 5.0 x 1.0 mm. These clasts contains JV type pyroxenes. The images of the PX-QUAD system suggest that pyroxene chemical compositions of Y82049 are divided into seven types: Pyx49(D1), Pyx49(D2), Pyx49(B), Pyx49(JV1), Pyx49(JV2), Pyx49(JV3) and Pyx49(Z). The range of chemical compositions of seven types of pyroxenes (Fig. 3d and Table 1d) in Y82049 is very wide (mg# =26 - 77). Because this sample includes olivines of

Fa_{50} and Fa_{36} , it is more likely to be a howardite. The characteristics of each pyroxene type can be described as follows:

Pyx49(D1) type. The Pyx49(D1) type pyroxenes are the most magnesian members ($mg\# = 77$) not only among the Y82049 pyroxene but also all samples observed in this paper, and their chemical compositions (Fig. 3d and Table 1d) are close to that of common diogenites. The pyroxenes of this type have no lamella observable by SEM (Fig.8a). No spinel was found in this type pyroxene.

Pyx49(D2) type. The pyx49(D2) type pyroxenes are the second most magnesian members among the Y82049 pyroxene. Their chemical compositions and exsolution textures (Fig. 3d and table 1d) are similar to Pyx39(D), Pyx92(D) and Pyx09(D). Thin augite lamellae less than $1\ \mu m$ wide are detected (Fig. 8b) by SEM. The lamellae are similar to typical (100) lamellae found in diogenitic clasts in howardites. They are too thin to be detected by EPMA. There is no spinel in this type of pyroxene.

Pyx49(B) type. The pyx49(B)-type pyroxenes have slightly more Fe-rich chemical compositions than other B-type pyroxenes in this paper (Fig. 3d and Table 1d). Many of them have blebs typical of Binda. Some pyroxenes have thick augite lamellae up to several microns, but the textures are severely disturbed by shock events (Fig.8c). This type of pyroxene can be crystallographically divided into Binda type and Moore County type of Delany's criteria as in the case of Y791439. One of this type of pyroxene (Fig.8d) includes FeS aggregates. The area is a triangle with $240\ \mu m$ edges. Other pyroxene has no FeS, making this portion very unique.

Pyx49(JV1) type.

The Pyx49(JV1)-type pyroxenes are a typical JV-type pyroxene (Fig. 3d and Table 1d) with exsolution lamellae several microns in width. One clast 280 μm x 600 μm in size includes this type pyroxenes and lath-shaped plagioclase (Fig.8e). They have thin (001) exsolution lamellae about 1 μm in width. The coexisting plagioclases have chemical compositions $\text{An}_{86}\text{-An}_{90}$. In this clast, there are chromites with variable Ti contents.

Pyx49(JV2) type.

The pyx49(JV2)-type pyroxenes are slightly more Fe-rich than those of Juvinas (Fig. 3d and Table 1d). They have thin exsolution lamellae, 3 μm in width with 6 μm interval (Fig.8f). Bulk chemical compositions are very Ca rich. They include chromites. One pyroxene has paring plagioclase $\text{An}_{90.5} - \text{An}_{91.5}$.

Pyx49(JV3) type.

The Pyx49(JV3) type pyroxenes are the most ferroan members not only among the Y82049 pyroxene but also all samples observed in this paper (Fig. 3d and Table 1d). The Pyx49(JV3)-type pyroxenes are more Fe rich than Juvinas. The width of thin augite lamellae is several μm (Fig.8g), and it is almost the same as that of host. This fact indicates that pyroxenes of this type have very Ca rich bulk chemical composition.

Pyx49(Z) type.

In this sample, zoned pyroxenes have no lamellae (Fig.8h) and exist mainly in large clasts. The chemical compositions of these pyroxenes (Fig. 3d) vary in mg# from 40 to 54, and their zoning seems to be produced in primary crystallization stage and not in Fe-Mg diffusion process. The largest clast in this PTS is composed of this type pyroxenes, and contains ilmenites. The chemical composition of coexisting plagioclase has wide

variations An_{77} - An_{92} .

Other minerals. The chemical compositions of most plagioclases in Y82049 fall in a limited range of anorthite content (An_{89} - An_{96}). The Pyx49 (JV)-type pyroxenes are coexisting with plagioclase having lower anorthite content than An_{90} . There are olivines (Fa_{50} and Fa_{36}), abundant chromites, and Fe-metals in the PTS.

3.2. Mineralogy and chemistry of cumulate eucrites

The author studied four cumulate eucrites: Medanitos, Nagaria, ALH85001 and Y791195. These cumulate eucrites are all unique in comparison with Moore County, Serra de Magé and Moama. For example, Medanitos is Ca poor. Nagaria is plagioclase rich. ALH85001 is Mg rich. Y791195 is Fe rich.

ALH85001

ALH85001 is a monomict eucrite with unusually magnesian pyroxene, similar to that in the Binda eucrite. It is brecciated but the original texture may have been equigranular. It is composed predominantly of pyroxene (49 %) up to 1.6 x 1.1 mm and plagioclase (50 %) up to 1.2 x 0.5 mm, with minor accessory phases (1 %) including chromite, troilite, and Fe-metal. The chemical compositions of the ALH85001 pyroxene are shown in Fig. 9 and Table 2. The ALH85001 pyroxenes look like the B-type pyroxenes of Y791439, but have slightly more Mg-rich in chemical compositions. Half of them have blebby augite typical of Binda, and others have thin ($< 1 \mu m$) augite

lamellae. The optical observations and Mg-rich chemical compositions suggest that these lamellae are on (100) as in the D-type pyroxenes. In spite of the textural variations, the chemical compositions of these pyroxenes are very uniform. Plagioclase compositions are also uniform ranging from An_{91} to An_{94} (Table 4).

Medanitos

Medanitos was described by Symes and Hutchison (1970), who classed it as a howardite because of its high content of Ca-poor pyroxene; however, Hutchison et al. (1977) reclassified it as a eucrite.

The original crystalline texture of Medanitos cannot be discerned because of its brecciated texture except for a few clasts. The largest pyroxene crystal in the studied Medanitos thin section reaches 1.75 mm in diameter, but most are much smaller fragments (<1 mm). The widths of exsolution lamellae of augite range from 1-10 μ m, and are thinner than Serra de Magé and Moore County. Medanitos is composed predominantly of pyroxene (43 %) and plagioclase (56 %), with minor accessory phases (1 %) including chromites, troilites, Ca-phosphates and silica polymorphs. The ratio of plagioclase to pyroxene in medanitos that we observed is not precise, because of the brecciated texture and poor quality of the PTS. The chemical compositions of the Medanitos pyroxene are almost uniform, as shown in Fig.9 and Table 2. Plagioclase compositions range from An_{93} to An_{95} (Table 3). In a few regions of the PTS, we recognize less brecciated portions where original crystallized textures are fairly well preserved. One such area 1.4 x 1.5 mm in size contains

round pyroxene 0.6 mm x 0.7 mm in size surrounded by plagioclase. But there is no difference between unbrecciated area and brecciated area in pyroxene chemistry and the width of lamellae.

Nagaria

Nagaria is a crystalline eucrite with a grain size (0.25 - 1.5 mm in diameter) that is smaller than Serra de Magé and Moore County. It is composed of pyroxene (40.9 %), plagioclase (58.8%) and minor accessory phases (0.3 %) including chromite and ilmenite. The chemical compositions of pyroxene are shown in Fig.9 and Table 2. And those of plagioclase are An90-An94 (Table 3). There are plagioclase-rich regions in all these eucrites and the grain boundaries are generally rounded. The exsolution and inversion texture of Nagaria has been reported previously (Takeda et al., 1983). The width of the augite lamellae (15 - 20 μm) (001) is less than Serra de Magé and Moore County. Blebby inclusions of augite between the thick lamellae, as typically seen in Serra de Magé, have not been observed in Nagaria.

Y791195

Y791195 is an unbrecciated eucrite chemically closer to ordinary eucrites (Takeda et al., 1988a), but it is more Mg-rich (mg# = 43) than the most Mg-rich non-Antarctic ordinary eucrites (Mason et al., 1979). Y791195 is composed of pyroxene (46.5 %), plagioclase (48 %) and relatively large amount of silica polymorph (5 %) with minor accessory phases (0.5 %)

including chromite and ilmenite. Y791195 shows a granular to microgabbroic texture. Short prismatic forms of plagioclase are rare, and parts of the crystalline texture are disturbed and recrystallized. The homogeneous plagioclase composition ($An_{89} - An_{93}$) indicates slower growth than ordinary eucrites. Y791195 has augite lamellae on (001) that are about $10\mu\text{m}$ thick at 20 to $40\mu\text{m}$ interval. They are thinner than lamellae commonly seen in cumulate eucrites. The moderate thickness of the augite exsolution lamellae are suggestive of slower cooling rates than for most ordinary eucrites. This eucrite fills a compositional gap between non-Antarctic cumulate eucrites and ordinary eucrites in the pyroxene quadrilateral.

4. Computer simulations

Estimation of equilibrium liquid

In order to make the magma differentiation trend of eucrites clear, the author calculated the activities of major elements (Fe, Mg, Ca) in equilibrium liquid coexisting with pyroxenes in the Y791439 polymict eucrite and some cumulate eucrites. For the calculation he adopted the modified Bottinga-Weill two-lattice melt model (Nielsen and Dungan, 1983), because it can eliminate most of variations in distribution coefficients caused by differences in melt composition. In this model, the melt is assumed to be made up of two independent quasi-lattice, network forming elements, composed of the components SiO_2 , NaAlO_2 , KAlO_2 , and the network modifying elements, composed of the free oxides of Fe, Mg, Ca, Ti, Cr and excess Al. The activities of each type of element are calculated separately. For example Fe activity is obtained by following equation: " Fe activity = Fe mol % / total mol% of network forming elements". We adopted Nielsen-Dungan crystal/liquid partition coefficients (Nielsen & Dungan, 1983). The equations for partition coefficient calculation are listed in Appendix I. They are not for cation mol% but for cation activities. The activities of three network-modifier elements (Fe, Mg, and Ca) in the liquid equilibrated with the pyroxenes in Y791439 are calculated and plotted in the Ca/Fe versus Mg/Fe (atomic ratio) diagram (Fig.10). Because partition coefficients change with respect to temperature, the data are plotted against temperature. Ca/Fe partition coefficient is so sensitive to temperature that the increase of Ca concentration in pyroxenes does not always mean increase of Ca in the equilibrium liquid.

On the other hand, since Mg/Fe partition coefficient is not so sensitive to temperature, we treated it as constant.

The liquid equilibrated with the D-type pyroxene (mg# = 68) has bulk composition (mg# = 38) similar to those of the ordinary eucrites. There is a high possibility that the D-type pyroxenes crystallized from the liquid which would solidify as an ordinary eucrite of the JV-type. The compositions of liquids equilibrated with Fe-rich pyroxenes (JV and MC type of Y791439) are more evolved than the bulk compositions of the ordinary eucrites. Such Fe-rich materials, however, have not been found in the meteorite collections.

For further discussion, we replot the calculated data on Fig.11, focusing on the mg# of liquid and solid phase. On this diagram the data of those cumulate eucrites which we observed and some well known eucrites are plotted. The bulk composition of the most Mg-rich Y7308 howardite is one of probable candidates for the parental liquid that crystallized diogenites and eucrites (Ikeda and Takeda, 1985) because it contains both surface rock and cumulate rock, and bulk compositions of ordinary eucrite are candidates for the evolved liquid compositions.

The results of this calculation show that the liquid coexisting with cumulate eucrites is too Fe rich, and there is no such Fe rich clasts in the HED achondrites. Simple maximum fractionation process could not produce cumulate eucrites. If we apply "partial melting model" (Stolper, 1977), the liquid produced from the cumulate eucrites is too Fe-rich for ordinary eucrite.

Considering the fact that even in the terrestrial gravity 25-50 vol% inter-cumulus liquid could remain between cumulate crystals (Anthony, 1990),

the author proposes another hypothesis: that cumulate eucrites contain large amount of inter-cumulus liquid. It is natural to have such liquid under low gravity field of the HED parent body, but after the liquid solidified as overgrowth of cumulus crystals and annealed, it is very difficult to identify whether there existed inter-cumulus phase or not initially.

For examining the efficiency of trapped liquid, computer simulation has been performed on fractional crystallization of mafic minerals with/without trapped liquid by a program written by the author. Mg#s of liquid and instantaneous solid (IS) in fractional crystallization process were calculated for each step of the fractionation. This simulation only handles Fe and Mg. For example, this program prepares hypothetical liquid composed of FeO and MgO. Then it calculates IS composition using Fe/Mg partition coefficient of pyroxene and fractionate hypothetical pyroxene composed of MgO and FeO with 0.1 vol % step of initial volume. This calculation is repeated until the liquid is used up. In the calculation, partition coefficient between pyroxene and liquid ($K_D=0.29$) is employed. In the early stage olivine also crystallized. In the equation: $(Mg/Fe)_{liq} = (Mg/Fe)_{sol} \times K_D$, partition coefficient (K_D) for olivine is about 0.31, and that for pyroxene is about 0.29. This difference does not affect the result severely. Initial mg# is taken from the Y7308 howardite bulk composition (Ikeda and Takeda, 1985) as a candidate for the bulk HED parent body crustal composition by the reason given above. The source code of this program is shown in "Appendix I".

The results of maximum fractionation of mafic elements are shown in Fig. 12a. In this process, crystals were completely separated from liquid.

When the mg# of fractionated pyroxene reaches to mg# of cumulate eucrite (mg# = 40-50), there is over 10 vol % liquid remained. And the remnant liquid has mg# over 80. The results of fractional crystallization with variable amount of trapped liquid are shown in Fig. 12b. In this case, Fe-rich cumulate eucrite can be produced without Fe rich liquid. When the amount of trapped liquid is around 50%, Fe-rich cumulate-eucritic (mg# = 45-55) could be produced from ordinary-eucritic liquid (mg# = 35-40).

As the mixing process of cooler solid and liquid proceeds, convection should be available, but it is not clear whether there is sufficient convection or not. Because the gravity on the HED parent body is very low, liquid trapping process is simpler in a low gravity parent body. In general, trapped liquid are used only for explanation of the REE distribution. Before this study, liquid trapping process had not been tested for the major elements (e.g. Fe and Mg) distribution, because it was difficult to simulate the crystal fractionation, but is reasonable for the major elements. If there are the variable amount of trapped liquid, many kinds of cumulate eucrite could be produced.

Magma differentiation simulation

For further discussion, fractional crystallization with trapped liquid has been simulated by adopting the modified Bottinga-Weill two-lattice melt model and Nielsen-Dungan crystal/liquid partition coefficients (Nielsen and Dungan, 1983). Saturated phases were determined by Longhi's liquidus boundary equations (Longhi and Pan, 1988). A program (MAGDIF.C) for examining physical processes such as crystal fractionation and solid-liquid remixing was

developed by the author. The source code of this program and explanation are shown in "Appendix I". Starting material was 1:10 mixture of Serra de Magé and Juvinas compositions. Because the author intended to show that the last stage magma can produce Fe-rich cumulate eucrites, he preferred low content of cumulate eucrite. This material was estimated as an analogue of 90% fractionated liquid in Fig.12B. A special trial was made to simulate the last stage of fractional crystallization on the HED parent body and produce ordinary eucritic liquid and cumulate eucrite by mixing 50% trapped liquid.

The results of this simulation are shown in Fig.13. The path of liquid compositions is shown in Fig.13 (a), crystallizing phases in Fig.13 (b), and the path of total solid phase in Fig.13 (c). Total solid composition is calculated by integrating instantaneously crystallizing phases and adding 50 vol% trapped liquid. The horizontal axis of three figure in Fig.13 show solid fraction in the oxygen unit. The value stands for the ratio of oxygen atoms in solid phase, and the values are almost the same as volume ratio, because most of the volume of magma and minerals is occupied by oxygen.

When the solid fractionation reaches to around 0.11, the $fe\#$ of liquid ($fe\# = 60$) approaches close to that of Juvinas ($fe\# = 57$), and the $fe\#$ of fractionated solid with trapped liquid ($fe\#=43$) is close to that of Serra de Magé ($fe\# = 42$). For $fe\#$ the result is in harmony with the calculation "fractional crystallization of mafic minerals with 50% trapped liquid" described in the previous paragraph. The liquid compositions are very close to Juvinas. It is natural because the starting materials are almost the same as the bulk composition of Juvinas. The ratio of cation of total solid is similar to Serra de

Magé, but the solid compositions were slightly more Si-poor than cumulate eucrites. This is caused by crystallization of olivine. Because olivine is a Si-poor mineral, solid phase become Si-poor during the olivine crystallization. When solid fraction reaches to 0.11, the solid phase is composed of 16 vol% of plagioclase, 34 vol% of olivine and 50 vol% of trapped liquid.

The calculated REE patterns of this model satisfy the observed ranges (Fig.14). For starting material, hypothetical ordinary eucritic liquid ($REE = 9 \times CCI$) is used. This starting material is that of pure ordinary eucrite but similar to the mixture of ordinary eucrite and cumulate eucrite of previous simulation, because the ratio of cumulate eucrite is very low. The partition coefficient data are after Drake and Weill (1975) for plagioclase/melt and Schnetzler and Philpotts (1970) for olivine/melt. The REE patterns are calculated by multiplying the starting material by partition coefficients. The enrichment of REE in liquid on crystallization is omitted because the amount of liquid is much greater than crystallized solid. The volume ratio of olivine and plagioclase obtained by MAGDIF is 34:16. Olivine has little influence on REE pattern because concentrations of REE in olivine are very low. The REE patterns are mainly determined by plagioclase and trapped liquid. Plagioclase contributes to Eu anomaly and the trapped liquid sets baseline. The REE pattern of total solid with 50% trapped liquid is close to that of Moore County. The REE pattern of fractionated solid with 10% trapped liquid (Fig.14) is close to Serra de Magé.

5. DISCUSSIONS

The remarkable textures of polymict eucrites

The pyroxenes of cumulate eucrites and ordinary eucrites show homogeneous chemical compositions of the host phase. The chemical homogeneity of pyroxene in cumulate eucrites may be the result of either slow igneous crystallization or thermal metamorphism that mobilized Fe, Mg and Ca and homogenized the originally zoned pyroxene. Homogenization of pyroxenes in ordinary eucrites has been proposed to be due to thermal metamorphism (Takeda and Graham, 1991). Many pyroxenes in polymict breccias in this study show chemical zoning. Pyx09(Z)-type and pyx49(Z)-type pyroxenes must be originally zoned pyroxenes, because there is Ca heterogeneity. For Fe-rich members, it is very difficult to distinguish whether the zoning was produced by original crystallization process or by diffusion in later stage. This is the first example to show the strong evidence that there is Mg-rich pyroxene with zoned Fe-rich rims by diffusion. The evidence is shown by one of pyx09(B)-type pyroxene (Fig.7b). The zoning profiles of pyx09(B) are shown in Fig.15 (a) (b). These two profiles were taken from opposite sides in a single pyroxene grain, and show both Fe zoning and augite exsolution lamellae. Because the diffusion coefficient of Fe is about hundred times larger than that of Ca (Miyamoto and Takeda, 1994), this zoning must have been produced after the formation of the augite lamellae. This zoning profile may be formed by a secondary heating event. Pyx09(D)-type pyroxenes have also zoned rim. The identical profiles suggest that these zoned rim must be produced by the same event with pyx09(b).

Another unique texture found in pyx92(JV)-type pyroxene, is the presence of second generation lamellae in the host and lamellae (Fig.6f). The profile of an exsolution lamella (Fig.14c) may indicate two stages cooling. In the same type pyroxene there is a pyroxene aggregate (Fig.6e), which may have formed in two stages. The first event may have produced small pyroxenes aggregate, and a second event may have produced the second stage lamellae.

The mechanisms for origin of the above unique textures are not clear. It can be, however, concluded that there are many local variations in thermal history on the HED parent body.

Magma differentiation trend of the HED parent body

The polymict eucrites and howardite in this study includes many kinds of cumulate eucrites and non-cumulate eucrites. Y791439 consists of three kinds of cumulate eucrites and one ordinary eucrite. Y791192 consists of five kinds of cumulate eucrites and one ordinary eucrite. Y82009 consists of three kinds of cumulate eucrites, one ordinary eucrites and zoned pyroxenes. Y82049 consists of three kinds of cumulate eucrites, three kinds of ordinary eucrites and zoned pyroxene. The fact that cumulate eucrites and ordinary eucrites are coexisting in the same PTS suggests that ordinary eucrites and cumulate eucrites existed in almost the same region of the HED parent body. In addition, many kinds of cumulate eucrites may have existed together in a close region. The surface of the HED parent body must be differentiated by magmatic process all over the body, because there is no chondritic clast nor

fragments of the primitive crust in these PTSs. There must be, however, regional differences in their differentiation process. Y791439 has only four types of pyroxene and Y82049 howardite have six types of equilibrated pyroxene and many zoned pyroxenes. The difference would be due to the extent of impact excavation and mixing. The breccia gathering clasts from a wider area have many kinds of pyroxenes.

How did pyroxenes with discontinuous chemical compositions form? To gain better understanding of the crystallization process, the author performed DTA work. The results are summarized in Appendix II. The author expected that many cycles of oversaturation and nucleation could lead to discontinuous crystallization in one differentiation process. But the experimental results suggest that it is hard to make oversaturated liquid in much slower cooling than our experimental run.

Cumulate eucrites have been regarded as cumulus from an evolved Fe-rich liquid, but there is no such Fe-rich quickly cooled clast in the HED meteorites. In Y82049 very Fe rich Juvinas-type pyroxenes with the mg# around 30 are observed. Liquid that has mg#=30 can produce only Mg-rich side of the cumulate eucrites. Calculation of equilibrium liquid coexisting with cumulate eucrites shows that there is no candidate for Fe-rich liquid in the meteorite collections up to date. The polymict breccias of this study also did not include glass resembling such an Fe-rich liquid. Sometimes small Fe-rich clasts are found in polymict breccias. For example, fayalite-silica clasts are reported in Y7803 (Ikeda and Takeda, 1985). Small amounts of Fe-rich magma, however, could not buffer the mg number during fractionation of

cumulate eucrites.

Some cumulate eucrites, especially Fe-rich ones (e.g., Y791195) may not be cumulus but slightly evolved liquid itself solidified slowly under an thick ordinary eucrite scurf (proto crust). The texture of Y791195 with equigranular finer grained pyroxene is consistent with this interpretation. However, there still remains one problem in this hypothesis. If such cumulate-eucritic liquid should exist, part of the liquid might flow over the surface and solidify as an Mg-rich lava-like eucrite. Y791438 has Mg-rich bulk pyroxene compositions ($\text{Ca}_8\text{Mg}_{50}\text{Fe}_{42}$) similar to Nagaria and Medanitos, and has quickly cooled texture of ordinary eucrite (Saiki et al., 1991). It may be a candidate for the Mg-rich liquid come up near the surface. There is no other eucrite which has both Mg-rich compositions and lava like texture.

Ikeda and Takeda (1985) studied details of lithic clasts and mineral fragments in the Y7308 Antarctic howardite and introduced trend B (Na-rich) magma as the source of cumulate eucrites. If the trend B magma should exist, it must be solidified as major components in polymict breccias. Fe rich clasts of trend B are present. In the Y791192 Juvinas-type pyroxene coexists with an Na-rich plagioclase ($\text{An}_{77}\text{-An}_{90}$). Y82009 and Y82049 also have Na-rich plagioclase, but the type of the paired pyroxene is unknown. Although there are many clasts including both pyroxene and plagioclase, in such clasts there is no Na-rich plagioclase coexisting with Mg-rich pyroxene. This fact suggests that there is no trend B magma, but in the last stage of fractional crystallization, Na-rich liquid is accumulated and Na-rich plagioclase crystallized. Computer simulation for fractional crystallization indicates that Na concentrated in

fractionated magma at the last stage. Since Ca also concentrated at the last stage, Na-rich plagioclase is not produced in computer simulation. In the condition of high-Ca and high-Na, phase boundary or mineral / melt partition coefficient may be changed.

In summary, the author proposed the trapped liquid model for the origin of cumulate eucrites and tested the model by computer simulation. One of the problems involved in disputes between the partialmelting model and the crystal fractionation model is that complex processes have to be introduced to explain all the facts known for the HED achondrites which cannot be proved or denied by simple experiments or theoretical studies. For testing hypotheses regarding complex physical processes such as fractional crystallization, mixing of trapped liquid, convection of crystallizing magma, etc., computer simulation is a powerful tool.

The results suggest that if the cumulate includes large amount of residual liquid (50%), cumulate eucrite ($Fe\# = \text{mean } 45-50$) could crystallize from ordinary eucritic liquid ($Fe\# = \text{mean } 60-65$). The mixing process of solid and liquid may have involved convection. But it is not clear whether there is sufficient convection or not, because the gravity on the HED parent body is very low. Therefore, the liquid trapping process is simpler. If there are the variable amounts of trapped liquid, many kinds of cumulate eucrites could be produced. It is remarkable that the variation of REE patterns could also be explained by the liquid trapping model.

Hereafter this kind of physical process such as mixing must be considered. In Y82009 and Y82049 there are many zoned pyroxenes. Some

of them are zoned by diffusion of iron from the matrix, but most of them are zoned in a crystallizing process, and they are not the Pasamonte-type and zoned from Mg-rich (mg# = ca. 35) side to Fe-rich side. Around such Mg-rich zoned pyroxene there are many equilibrated Mg-rich pyroxenes in the same PTS, indicating that a mixing event such as an impact mixing occurred in the course of crustal formation when the crust was still hot.

In the computer simulation, the mixing liquid between Juvinas and Serra de Magé resulted in crystallization of olivine at the first stage. It looks strange because there is no olivine found in Juvinas and Serra de Magé. Stolper's melting experiments (Stolper, 1977), however, demonstrate that the first mineral phase to crystallize from cumulate eucrite melt is olivine, and the olivine reacts to form pyroxene at lower temperature.

We have to admit that the accuracy of the results of computer simulation is still beyond application to a complex natural process. For example, in the estimation of crystallizing minerals, the author calculated the compositions of equilibrium mineral and equilibrium temperature from a given liquid. In fractional crystallization simulation, the temperature often jumps up in case the crystallizing mineral changes, where liquid path entered between liquidus and solidus. In such case, the present theory gives us no answer for chemical compositions and temperature. A new liquid model is also needed. The two lattice melt model is very useful but when the chemical composition approaches close to endmember the accuracy drops down. After all, simulation work tells the scientists faults of his theory. For understanding the magma changing in chemical composition, the study of dynamic process is

indispensable. Especially, reaction process of olivine is very important for better understanding of magma differentiation. For the dynamic crystallization study involving reaction between crystallized phase and liquid the author proposed again the application of DTA as are shown in Appendix II.

In order to make the magma differentiation process clear, we must pay more attention to this olivine reaction process. The calculated cumulate eucrite has slightly Si-poor compositions. This is an effect of crystallization of an olivine component. The timing of crystallization and reaction of olivine must be examined in future work.

The origin of cumulate eucrites deduced from pyroxene differentiation trends

The presence of the JV-type pyroxene in Y791439, Y791192, Y82009 and Y82049 suggests that ordinary eucrite located next to the cumulate eucrites. Therefore, we must consider the genetic link between ordinary eucrite and cumulate eucrite. With our renewed interest in the cumulate eucrites, four individual specimens in this study are interpreted in terms of magma differentiation.

The modal data (Table 4) suggest the possibility that large amounts of the B-type cumulate eucrites exist deep in the HED parent body. Assuming that these types constitute a layered crust or cumulate piles and they are equally sampled by the excavation, we suggest that large amount of cumulate eucrites, especially B-type, are located at a region between diogenites and ordinary eucrites. This interpretation gives further support for an idea that cumulate eucrites are link materials between diogenites and ordinary eucrites.

Previously, it is thought that the B-type cumulate eucrite is a rare component of the HED parent body, but considering the modal data and the fact that ALH85001 has the B-type pyroxenes, we conclude that the B-type cumulate eucrites may be common components at the deep region of the crust of the HED parent body.

ALH85001 may be one of the most conventional cumulate eucrite. Its Mg-rich compositions can be produced from ordinary eucritic liquid by maximum fractionation. It should be located at the lowest layer of the eucrite crust because it has chemical compositions as maximum fractionation product. So the B-type eucrite is rare in monomict eucrite.

Medanitos may be cumulus from an Fe-rich liquid like Nuevo Laredo or may be slightly evolved liquid itself. When we produce a cumulate eucrite with maximum fractionation of ordinary eucritic liquid, the compositions of Medanitos locates the most Fe-rich side. The REE pattern of Medanitos shows that this sample is a cumulate rock (Kiesl et al., 1978). The relatively thin exsolution lamellae suggested that it was cooled near the surface probably by excavation from depth by an impact. The heterogeneity of texture may suggest it was originally a polymict breccia. But thermal annealing erased the chemical heterogeneity. Kiesl et al. (1978) mentioned "*The pyroxene (modal abundance of 70-75%) shows a variable composition ranging in Ca content between $Ca_1Mg_{62}Fe_{37}$ and $Ca_{43}Mg_{44}Fe_{13}$ and an Al content up to 20% Al_2O_3* " and "*... the variation wideness of the pyroxene between En_{43} to En_{61} . The presence of zoning of the pyroxenes suggests that no further metamorphism took place.*" We think what they call zoning is incomplete resolution of

exsolution due to thin lamellae width, because they choose lamella and host chemical compositions as endmembers of pyroxene variation. We suspect the existence of Al rich pyroxene. The mixture of 50 % of the host pyroxene compositions and 50 % of the plagioclase compositions almost agree with their Al-rich pyroxene compositions. Al-rich pyroxenes must be glass or boundary between pyroxene and plagioclase. Our results suggest that Medanitos suffered from thermal annealing.

Nagaria may be slightly evolved liquid itself but most likely to be a cumulus with a large amount of trapped liquid. If it is evolved liquid itself, there should be a cumulus more Mg-rich than the B-type in the B-type cumulate eucrite. So we prefer the trapped liquid model for Nagaria.

Based on its major element chemistries and non-preferred orientation texture, the author suggested that Y791195 is a good candidate for evolved liquid itself. It may be an Mg-rich non-cumulate eucrite. The REE pattern of Y791195, however, shows that it is similar to cumulate eucrites in its bulk chemistry, and is intermediate between Serra de Magé and Moore County in the REE contents (Mittlefehldt and Lindstrom, 1993, Warren and Kallemeyn, 1992). In view of the trapped liquid model, the presence of Fe-rich cumulate eucrite is acceptable, but its low REE contents cannot be explained at present.

6. CONCLUSIONS

Among many models proposed to explain the origin of eucrites, none of them could explain the variation of eucrites especially cumulate eucrites without hypothetical materials. In this work, four polymict breccias and four cumulate eucrites have been investigated to check the systematic variation of pyroxenes in eucrites by employing chemical mapping system constructed by the author. In order to explain the chemical variations of eucrites without hypothetical phase, three kinds of computer simulation for testing the model were constructed and performed. The magmatic system on the HED parent body is well suited for computer simulation, because the HED materials differentiated from chondritic materials by simple processes such as partial melting and fractional crystallization at low pressure without water and Fe^{3+} free.

To simulate the differentiation path of the HED magma, the activities of major elements (FeO , MgO , CaO) in equilibrium liquid coexisting with pyroxenes in the Y791439 polymict breccia and some cumulate eucrites were calculated using partition coefficient between pyroxene and liquid with modified two lattice melt model of Nielsen and Dungan (1983). To test "liquid trapping model" proposed by the author, he made a simulation program for the fractional crystallization of mafic elements. Mg number (mg\#) ($=\text{Mg} \times 100 / (\text{Mg} + \text{Fe})$) of liquid and instantaneous solid (IS) in the fractional crystallization process were calculated. In order to test the phase relation and compositional changes of melt and minerals, the author made a simulation program "MAGDIF" was made by a method proposed by Longhi and Pan (1988) and

developed by the author for handling trapped liquid and for educational use.

The results are summarized as follows:

- (1) The existence of mixtures of ordinary eucrite and cumulate eucrites in polymict breccias Y791439, Y791192, Y82009 and Y82049 indicate that ordinary eucrite and several kinds of cumulate eucrites existed together in a close region of the HED parent body.
- (2) Entire survey on the available PTS's of polymict eucrites revealed that no remnants of chondritic source materials, nor the residue of partial melting have been mixed.
- (3) There are variations in the thermal history in the pyroxenes in cumulate eucrite clasts. Especially, one pyroxene in Y82009, with Fe/Mg zoning at the rims despite augite exsolution lamellae, is the first evidence for secondary diffusion after lamellae formation.
- (4) The equilibrium calculation shows that the liquid coexisting with cumulate eucrite are too Fe rich. All previous models producing cumulate eucrites needs such hypothetical Fe-rich liquid.
- (5) In order to explain the origin and variations of cumulate eucrites with no hypothetical liquid, the author proposed "trapped liquid model". The model proposes that some cumulate eucrites may be produced by fractional crystallization with large amount (40-50%) of trapped liquid.
- (6) The Mg-Fe fractional crystallization simulation indicated that if the cumulus includes large amount of residual trapped liquid (40-50%), a cumulate eucrite (Fe# = mean 45-50) could crystallize from ordinary eucritic liquid (Fe# = mean 60-65).

(7) The variation of many cumulate eucrites can be reproduced by the variable amounts of trapped liquid.

(8) A computer simulation by "MAGDIF" showed that the ratio of cation produced by 50 vol% trapped liquid are similar to cumulate eucrite, but slightly more Si-poor than cumulate eucrites because of olivine in cumulus phase.

(9) The first phase crystallized from starting magma is olivine, but there is no olivine in cumulate eucrites and most of polymict eucrites. It is very important to make the olivine reaction process clear.

(10) During the course of simulation of crystallization, it was found that, when liquid path entered between liquidus and solidus in crystallization process, the present theory gives us no answer for chemical compositions of crystallizing mineral.

(11) The calculation of REE distribution suggested that the variation of REE level of cumulate eucrites can also be reproduced by mixing crystallized olivine in early stage, plagioclase and 10 - 50 vol% trapped liquid.

The variations of pyroxenes in eucrites can be explained by simple process of "liquid trapping". The efficiency of simulation work has been demonstrated for testing the model.

ACKNOWLEDGMENTS

The author thanks the staff of the National Institute of Polar Research, the British Museum (Natural History), and Meteorite Working Group (MWG) in the U. S. for providing him with meteorite samples. He is indebted to Mr. O. Tachikawa for his assistance during the SEM, EDS, and CMA work, Mr. H. Yoshida and Prof. M. Miyamoto for his assistance during the EPMA work, and Dr. J. Longhi for giving him useful information in simulation work. The author thanks Dr. T. Ozawa for helpful advice, and Drs. T. Tagai and H. Horiuchi for allowing him to operate their Think C and MS-C language. He also thanks Prof. H. Takeda and P.H. Warren for valuable suggestions and discussions for this study. This work is supported in part by Fellowships of the Japanese Society for the Promotion of Science for Japanese Junior Scientists.

REFERENCES

- Anthony R.P. (1990) Principles of igneous and metamorphic petrology. Prentice Hall, 498pp.
- Binzel R.P. and Xu S. (1993) Chips off of asteroid 4 Vesta: Evidence for the parent body of basaltic achondrite meteorites, *Science* 260, 186-191.
- BVSP (Basaltic Volcanism Study Project) (1981) Basaltic Volcanism on the Terrestrial Planets. Pergamon, New York. 1286pp.
- Consolmagno G. J. and Drake M. J. (1977) Composition and evolution of the eucrite parent body: Evidence from rare earth elements. *Geochim. Cosmochim. Acta*, 41, 1271-1282.
- Delaney J. S., Prinz M. and Takeda H. (1984) The polymict eucrites. *Proc. Lunar Planet. Sci. Conf. 15th*, C251-C288.
- Duke M. B. and Silver L. T. (1967) Petrology of eucrites, howardites and mesosiderites. *Geochim. Cosmochim. Acta*, 31, 1637-1665.
- Drake M. J. and Weill D. F. (1975) Partition of Sr, Ba, Ca, Y, Eu²⁺, Eu³⁺, and other REE between plagioclase feldspar and magmatic liquid: an experimental study. *Geochim. Cosmochim. Acta* 39, 689-712.
- Dreibus G. and Wänke H. (1979) The bulk composition of the moon and the eucrite parent body. *Proc. Lunar Sci. Conf. 8th*, 211-227.
- Gaffey M.J. (1993) Forging an asteroid-meteorite link, *Science* 260, 167-168.
- Harlow G. E., Nehru C. E., Prinz M., Taylor G. J. and Keil K. (1979) Moama and Moore County. *Earth Planet. Sci. Lett.*, 43, 173-181.
- Hewins R.H. and Newsom H.E. (1988) Igneous activity in the early solar system. in "Meteorites and the early solar system", Kerridge J.F. and Matthews M.S. ed., The University of Arizona Press, Tucson, 73-101.

- Hutchson, R., Bevan A.W.R., and Hall J.M. (1977) Appendix to the Catalogue of Meteorites with Special Reference to Those Represented in the Collection of the British Museum (Natural History).p149.
- Ikeda Y. and Takeda H. (1985) A model for the origin of basaltic achondrites based on the Yamato 7308 howardite. Proc. Lunar Planet. Sci. Conf. 15th, in J. Geophys. Res., 90, C649-C663.
- Kiesl W., Weinke H. H., and Wichtl M.(1978) The Medanitos meteorite. Meteoritics., 31, 513-516.
- Longhi J. and Pan V. (1988) Phase equilibrium constraints on the Howardite-Eucrite-Diogenite association. Proc. Lunar Planet. Sci. Conf. 18th, pp. 459-470.
- Mason B. (1962) Meteorites (New York: Wiley), 116-119.
- Mason B., Jarosewich E. and Nelen J. A. (1979) The pyroxene-plagioclase achondrites. Smithsonian Contrib. Earth Sci., 22, 27-45.
- Mittlefehldt D.W. and Lindstrom M.M. (1993) Geochemistry and petrology of a suite of the Yamato HED meteorites. Proc. NIPR Symp. Antarct. Meteorites, 6,268-292,1993.
- Miyamoto M. and Takeda H. (1994) Thermal history of lodranites Yamato 74357 and MAC88177 as inferred from the chemical zoning of pyroxene and olivine. Journal of Geophys. Res., 99, 5669-5677.
- Mori H. and Takeda H. (1981) Evolution of the Moore County pyroxenes as viewed by an analytical transmission electron microscope (ATEM)., (abstract). Meteoritics, 16, 362-363.
- Nakamura Y. and Kushiro I. (1970) Compositional relations of coexisting orthopyroxene, pigeonite, and augite in a tholeiitic andesite from Hakone Volcano. Contr. Mineral. Petrol. 26, 265-275.

- Nielsen R.L. and Dungan M.A.(1983) Low pressure mineral-melt equilibria in natural anhydrous mafic systems. *Contrib. Mineral.Petrol.* 84, 310-326.
- Nyquist L.E., Takeda H., Bansal B.M., Shih C.-Y., Wiesmann H., and Wooden J.L. (1986) Rb-Sr and Sm-Nd internal isochron ages of a subophitic basalt clast and a matrix sample from the Y75011 eucrites. *J. Geophys. Res.*, 91, 8137-8150.
- Saiki K., Takeda H., and Tagai T. (1991) Zircon in magnesian, basaltic eucrite Yamato 791438 and its possible origin. *Proc.Lunar and Planet. Sci.* 21st, 341-349.
- Saiki K., Yamaguchi A., and Takeda H.(1992) New chemical mapping technique for analysis of pyroxenes in polymict breccias and application to some eucrites (abstract). *Lunar Planet. Sci.* XXIII . pp.1201-1202.
- Schnetzieler C. C. and Philpotts J. A. (1970) Partition coefficients of rare-earth elements between igneous matrix material and rock-forming mineral phenocrysts-II. *Geochim. Cosmochim. Acta* 34, 331-340.
- Symes R.F. and Hutchison R. (1970) Medanitos and Putinga, two South American meteorites. *Min. Mag.*,vol.37, p.721.
- Stolper E. (1977) Experimental petrology of eucritic meteorites. *Geochim. Cosmochim. Acta*, 41, 587-611.
- Takeda H. (1979) A layered crust model of a howardite parent body. *Icarus* 40, 445-470.
- Takeda H. (1986) Mineralogy of Yamato 791073 with reference to crystal fractionation of the howardite parent body. *Proc. Lunar and Planet. Sci. Conf. 16th.*, 91, *J.Geophys.Res.*, D355-D363.

- Takeda H. and Graham A.L. (1991) Degree of equilibration of eucritic pyroxenes and thermal metamorphism of the earliest planetary crust. *Meteoritics*, 26, 129-134.
- Takeda H. and Hidaka O. (1989) Association of diogenites and cumulate eucrites in Yamato 791439 and their genetic link (abstract). *Meteoritics*, 24, p.331
- Takeda H. and Mori H. (1985) The diogenite-eucrite links and the crystallization history of a crust of their parent body. *Proc. Lunar Planet. Sci. Conf. 15th*, in *J. Geophys. Res.*, 89, c636-c648.
- Takeda H, Miyamoto M., Ishii T., and Reid A. M. (1976) Characterization of crust formation on a parent body of achondrites and the moon by pyroxene crystallography and chemistry. *Proc. Lunar Sci. Conf. 7th.*, 3535-3548.
- Takeda H., Miyamoto M., Duke M.B., and Ishii T. (1978) Crystallization of pyroxene in lunar KREEP basalt 15386 and meteoritic basalts *Proc. Lunar Planet. Sci. Conf. 9th*, 1157-1171.
- Takeda H., Mori H., Delaney J. S., Prinz M., Harlow G. E. and Ishii T. (1983) Mineralogical comparison of Antarctic and non-Antarctic HED (howardites -eucrites-diogenites) achondrites. *Mem. Natl. Inst. Polar Res., Spec. Issue 30*, 181-205. *Natl. Inst. Polar Res., Tokyo*.
- Warren P. H. (1985) Origin of howardites, diogenites and eucrites: A mass balance constraint. *Geochim. Cosmochim. Acta*, 49, 577-586.
- Warren P.H. and Kallemeyn G.W. (1992) Further evidence for geochemical diversity, and possible bimodality, among cumulate eucrites. (abstract) *Meteoritics*, 27, 303-304.
- Yanai K. and Kojima H., comp. (1987): *Photographic Catalog of Antarctic Meteorites*. Tokyo, Natl. Inst. Polar Res., 298p

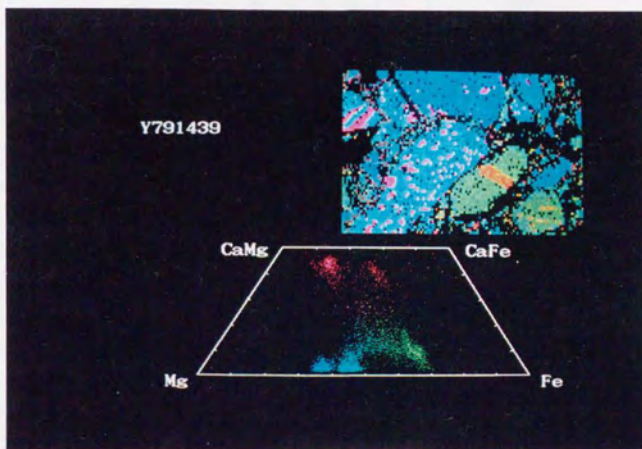
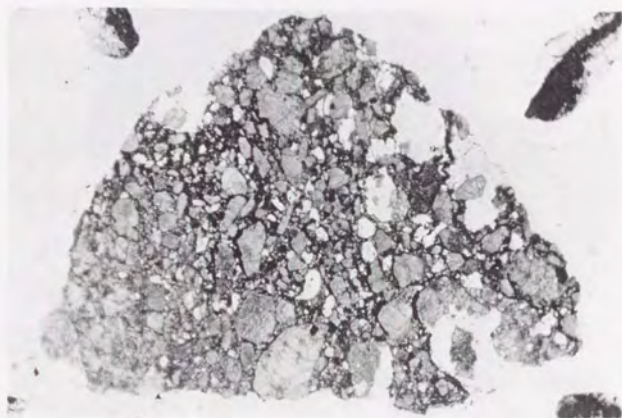
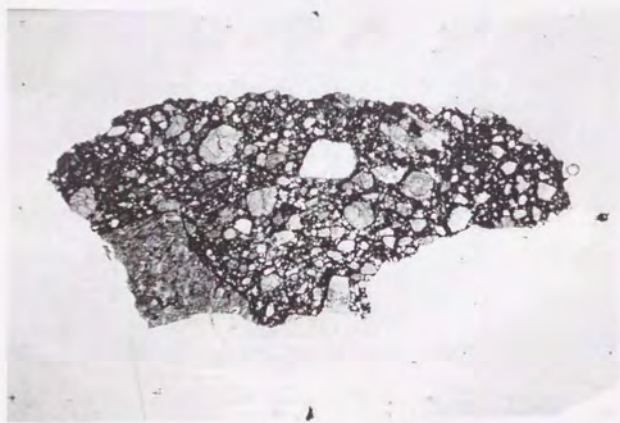


Fig.1 Sample image of the PXQUAD system for Y791439. Three kinds of pyroxenes are detected in this area.

Fig.2 Photomicrograph of (a) Y791439, (b) Y791192, (c) Y82009 and
(d)Y82049. Width is 3.3 mm.



(a) Y791439



(b) Y791192

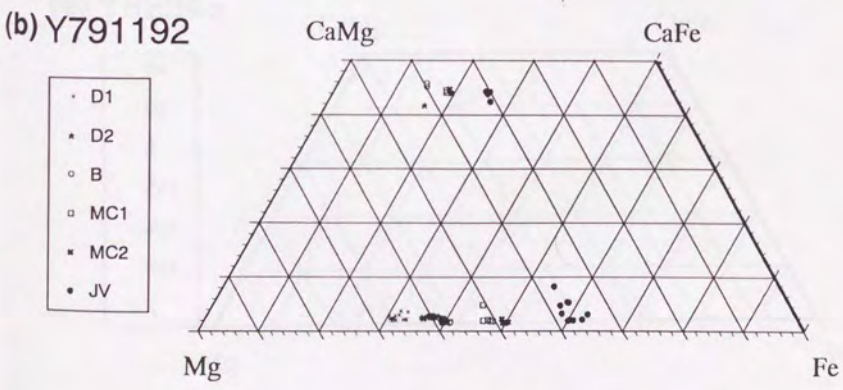
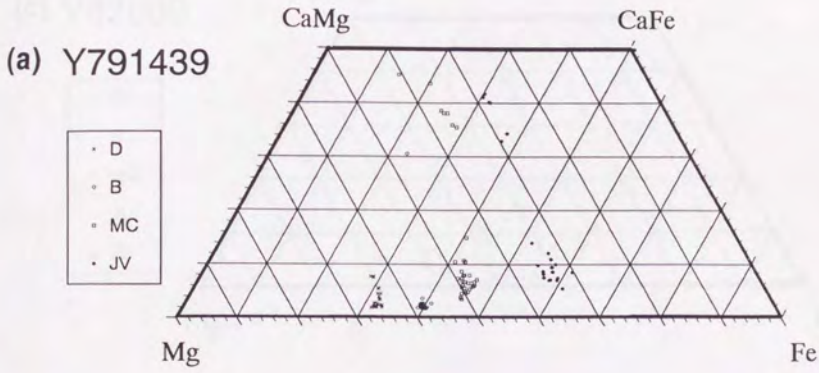


(c) Y82009

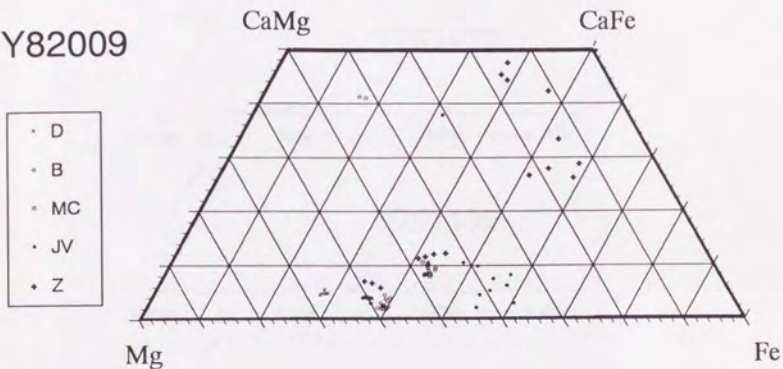


(d) Y82049

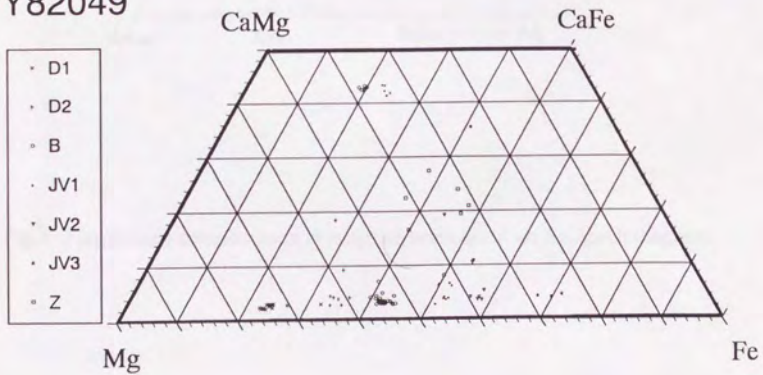
Fig.3 Pyroxene quadrilaterals of each type of the pyroxene in (a) Y791439,
 (b) Y791192, (c) Y82009 and (d) Y82049.



(c) Y82009



(d) Y82049



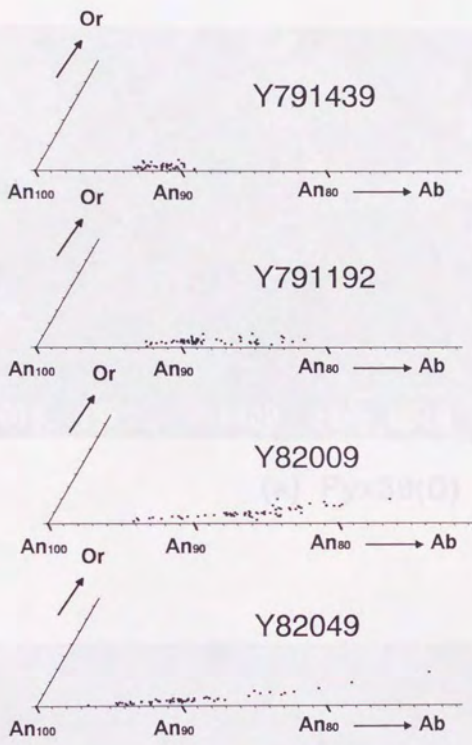
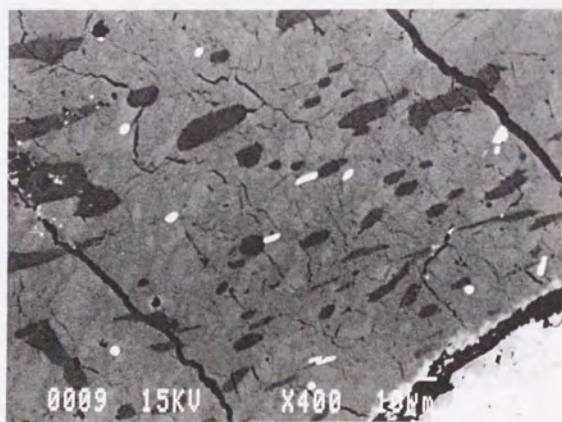


Fig.4 Plagioclase compositions of polymict breccias in an An-Ab-Or diagram.

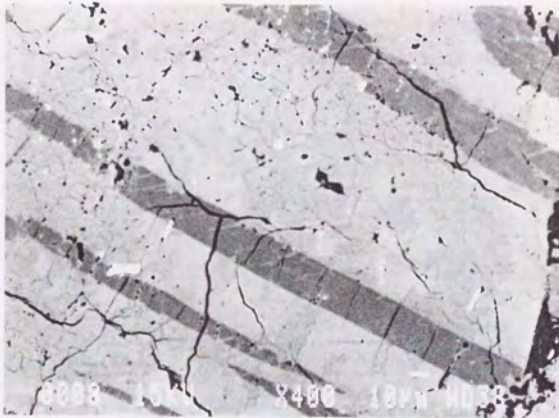
Fig.5 Backscattered electron images of typical pyroxenes in Y791439.



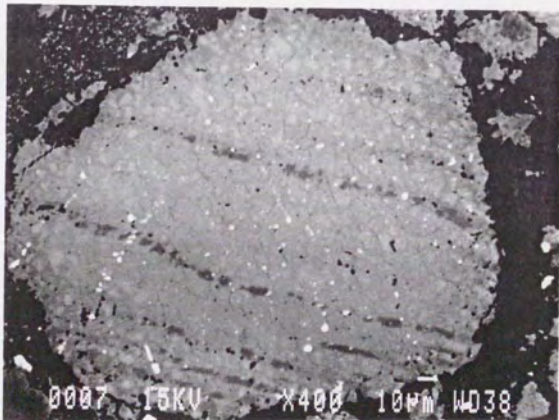
(a) Pyx39(D)



(b) Pyx39(B)

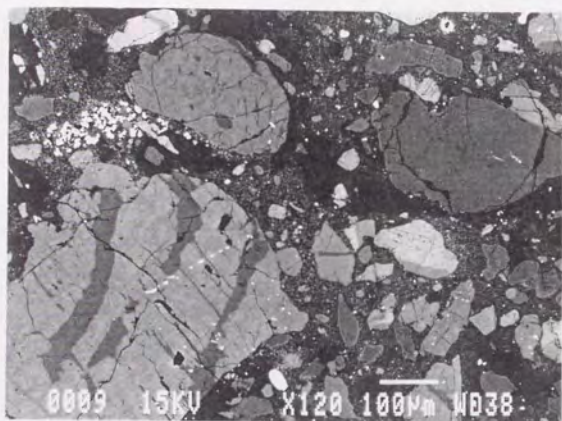


(C) Pyx39(MC)

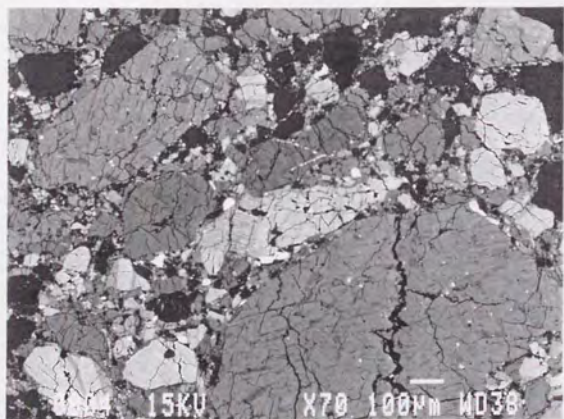
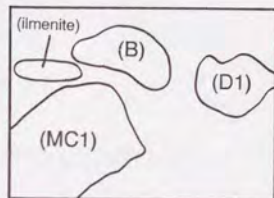


(d) Pyx39(JV)

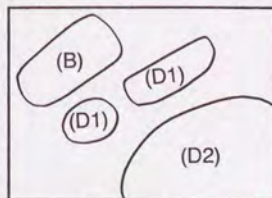
Fig.6 Backscattered electron images of typical pyroxenes in Y791192.

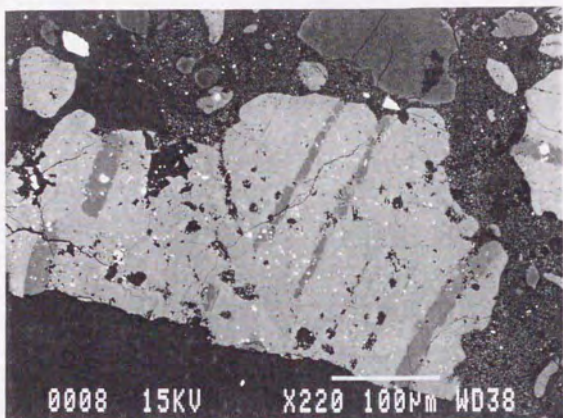


(a)

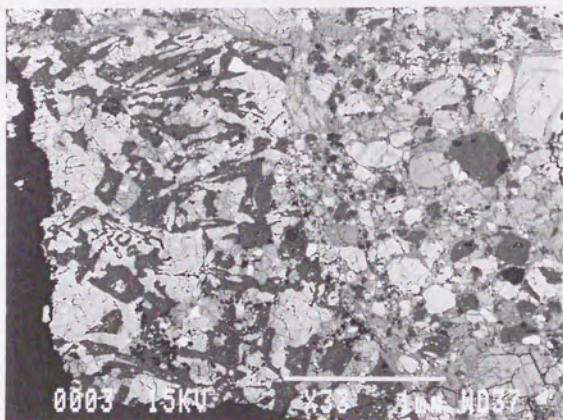


(b)

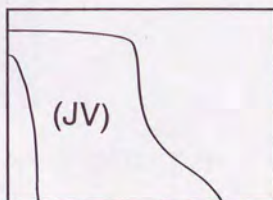


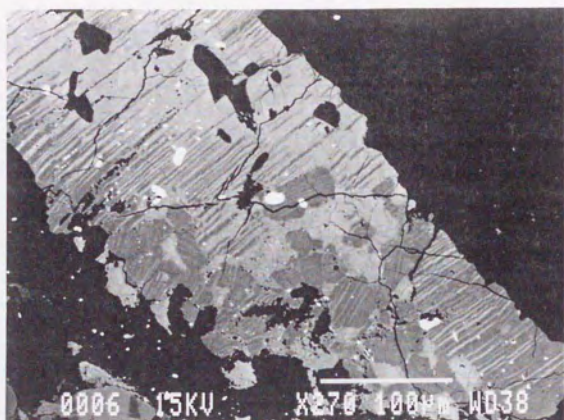


(c) Pyx92(MC2)

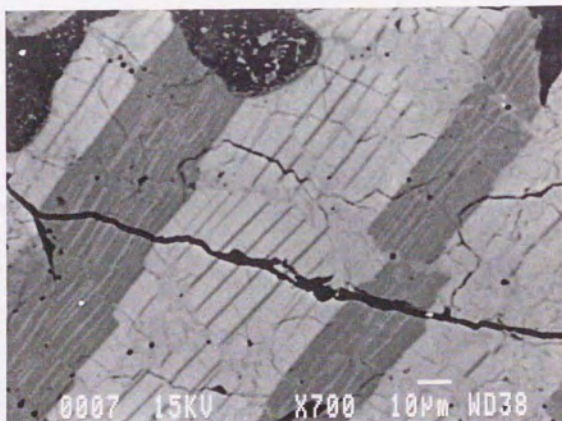


(d)



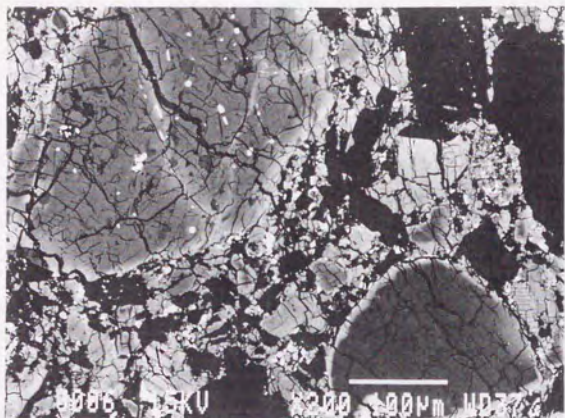


(e) Pyx92(JV)

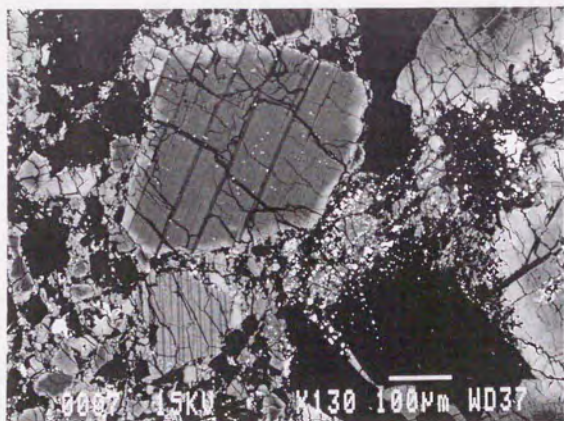
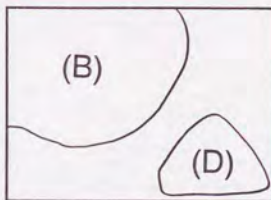


(f) Pyx92(JV)

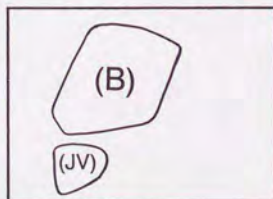
Fig.7 Backscattered electron images of typical pyroxenes in Y82009.

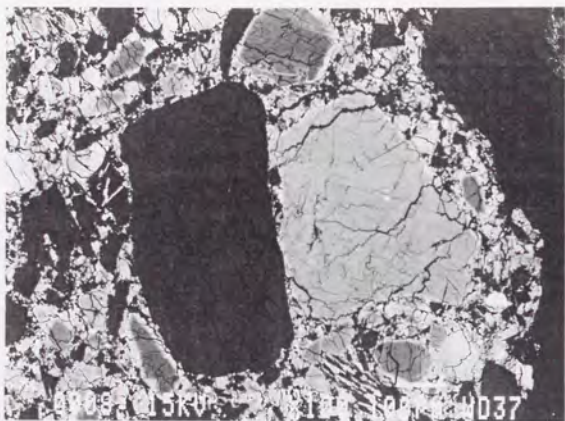


(a)

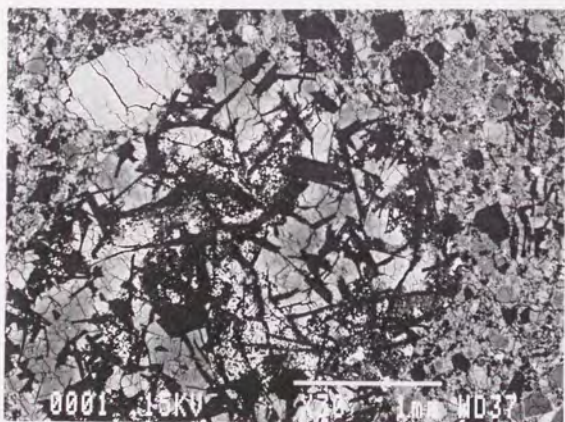
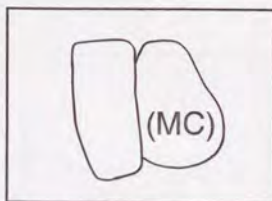


(b)

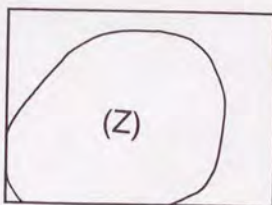


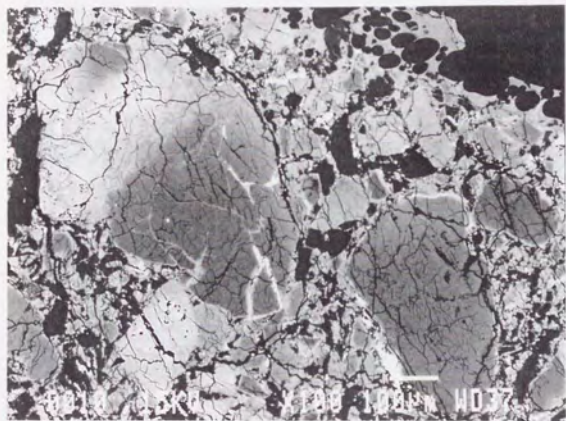


(c)



(d)





(e)

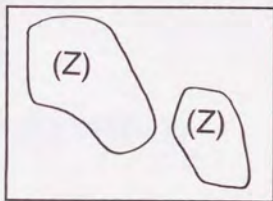
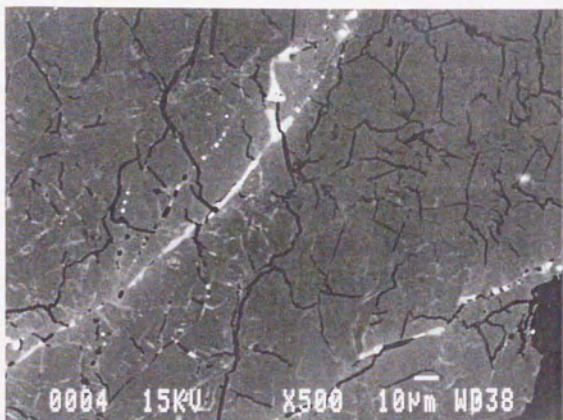
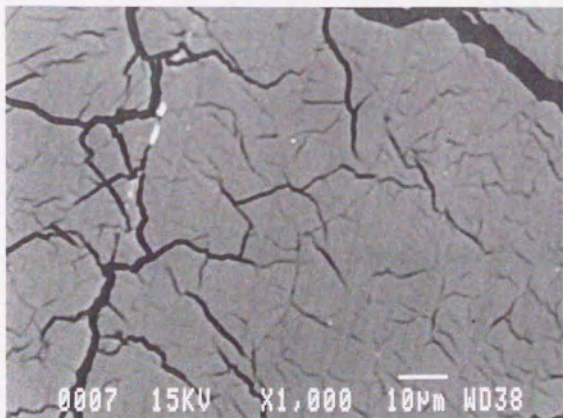


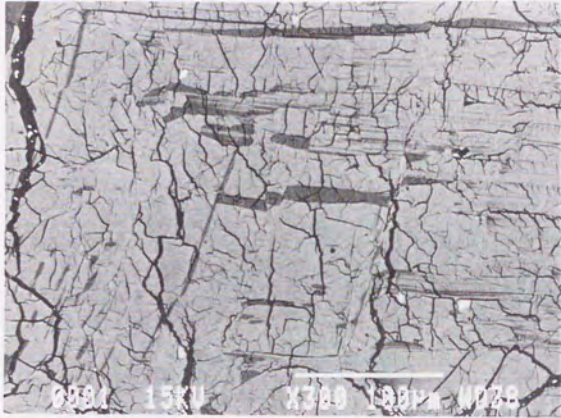
Fig.8 Backscattered electron images of typical pyroxenes in Y82049.



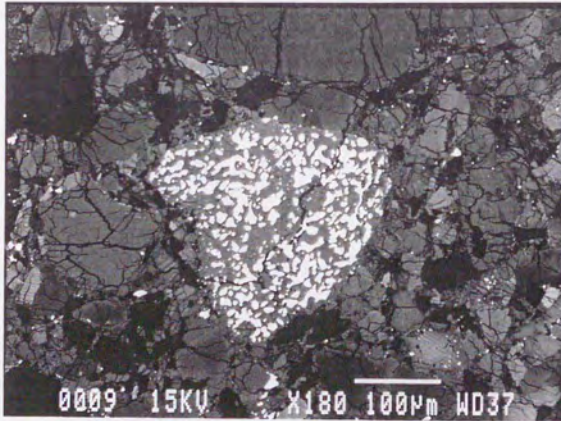
(a) Pyx49(D1)



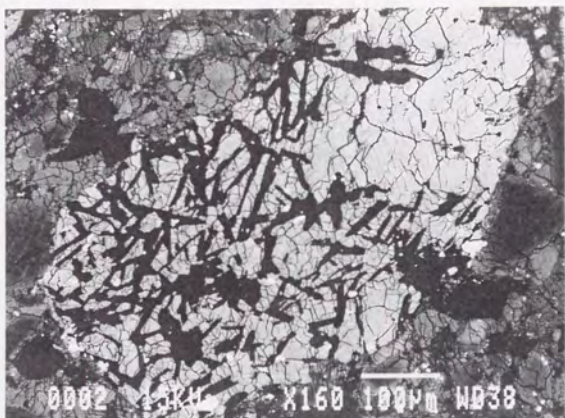
(b) Pyx49(D2)



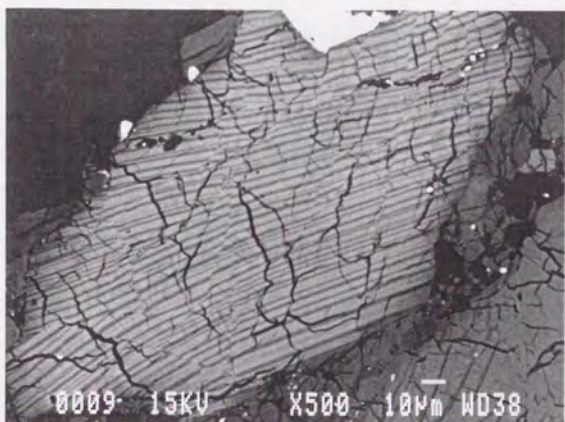
(c) Pyx49(B)



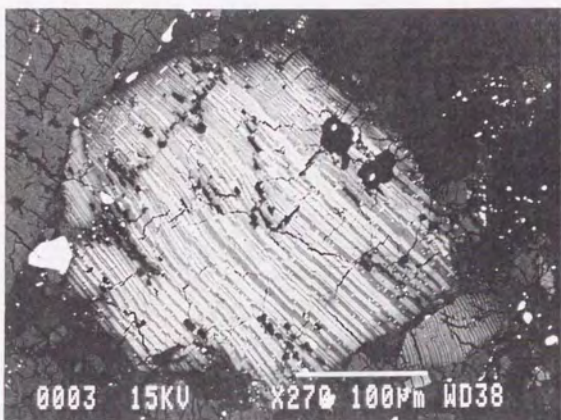
(d) FeS in Pyx49(B)



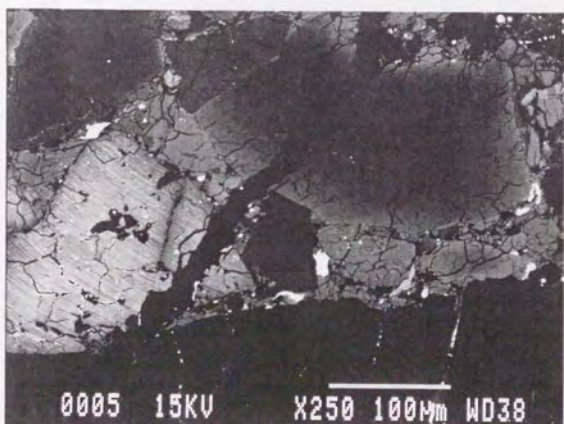
(e) Pyx49(JV1)



(f) Pyx49(JV2)



(g) Pyx49(JV3)



(h) Pyx49(Z)

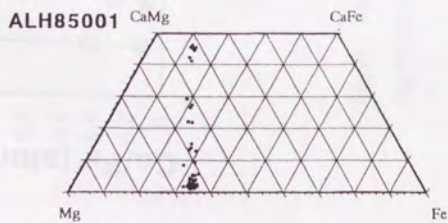
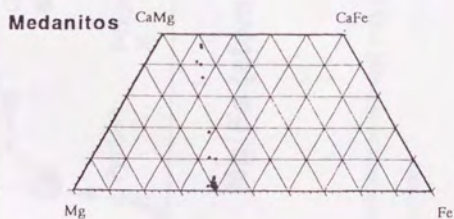
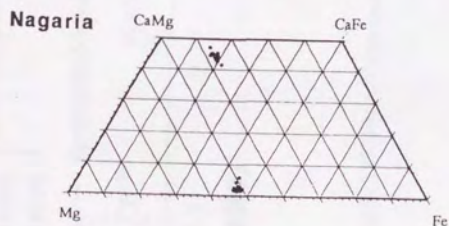
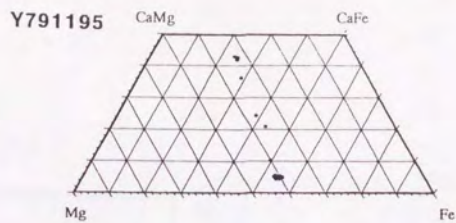


Fig.9 Pyroxene quadrilaterals of four cumulate eucrites. Medanitos, Nagaria, ALH85001 and Y791195.

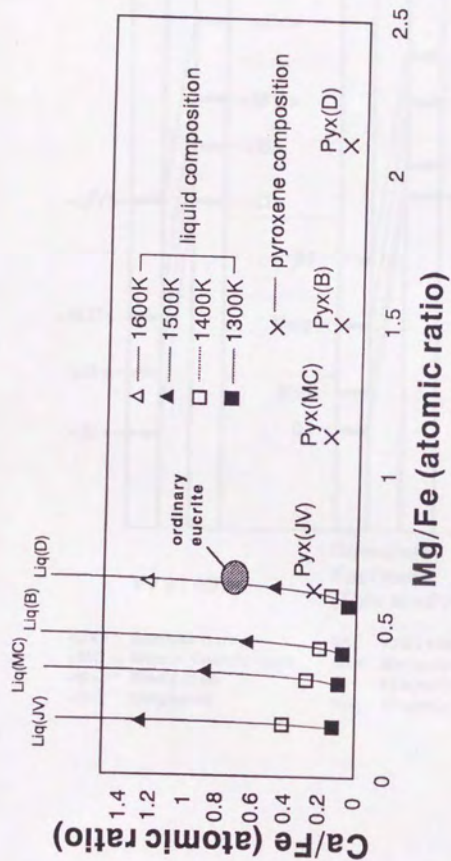


Fig. 10 Hypothetical liquids equilibrated with pyroxenes in Y791439 on Ca/Fe versus Mg/Fe atomic ratio diagram.

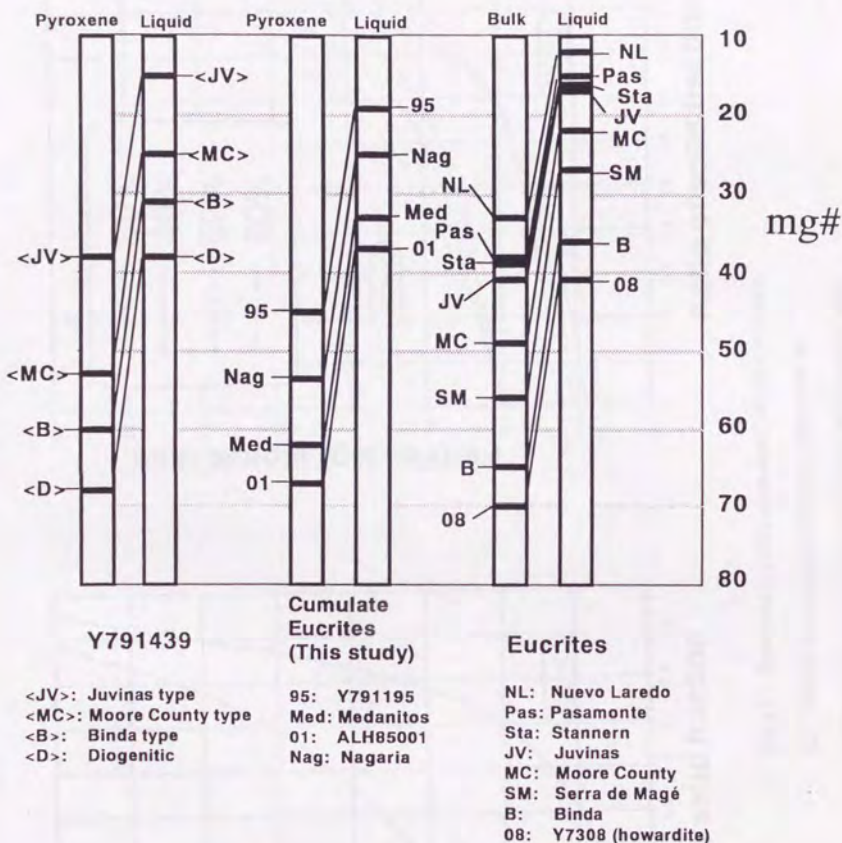
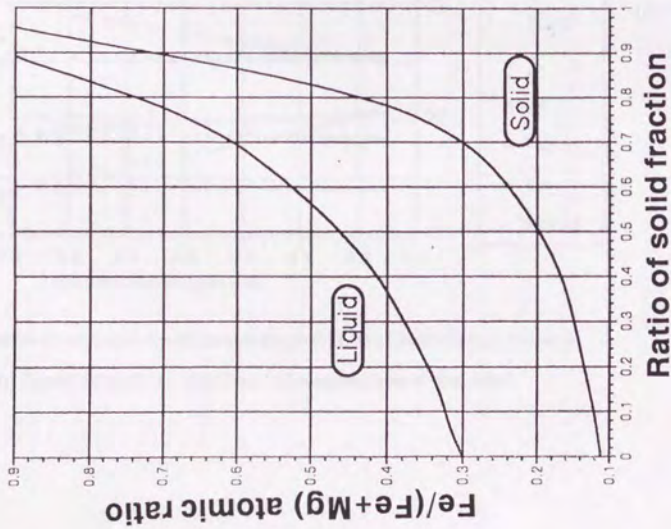


Fig. 11 mg# chart of eucrites and estimated liquids equilibrated with their pyroxene or bulk composition. The chemical composition data of Y791439, ALH85001, Medanitos, Nagaria and Y791195 are obtained in this study. Bulk chemical compositions of Y7308 is taken from Ikeda & Takeda (1985) and those of the other meteorites are taken from BVSP (1981). The left side columns show observed chemical compositions. The right side columns show calculated equilibrium liquid compositions.

(a)



(b)

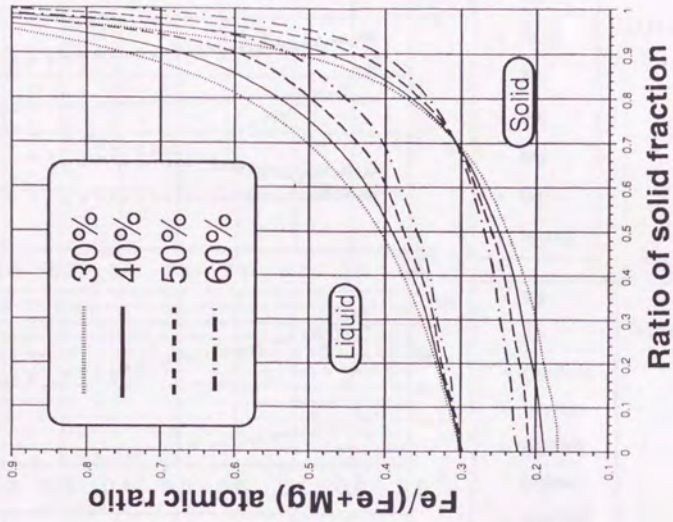


Fig.12 Fractional crystallization model of mafic minerals.

(a) The case of maximum fractional crystallization.

(b) The case of fractional crystallization with trapped liquid.

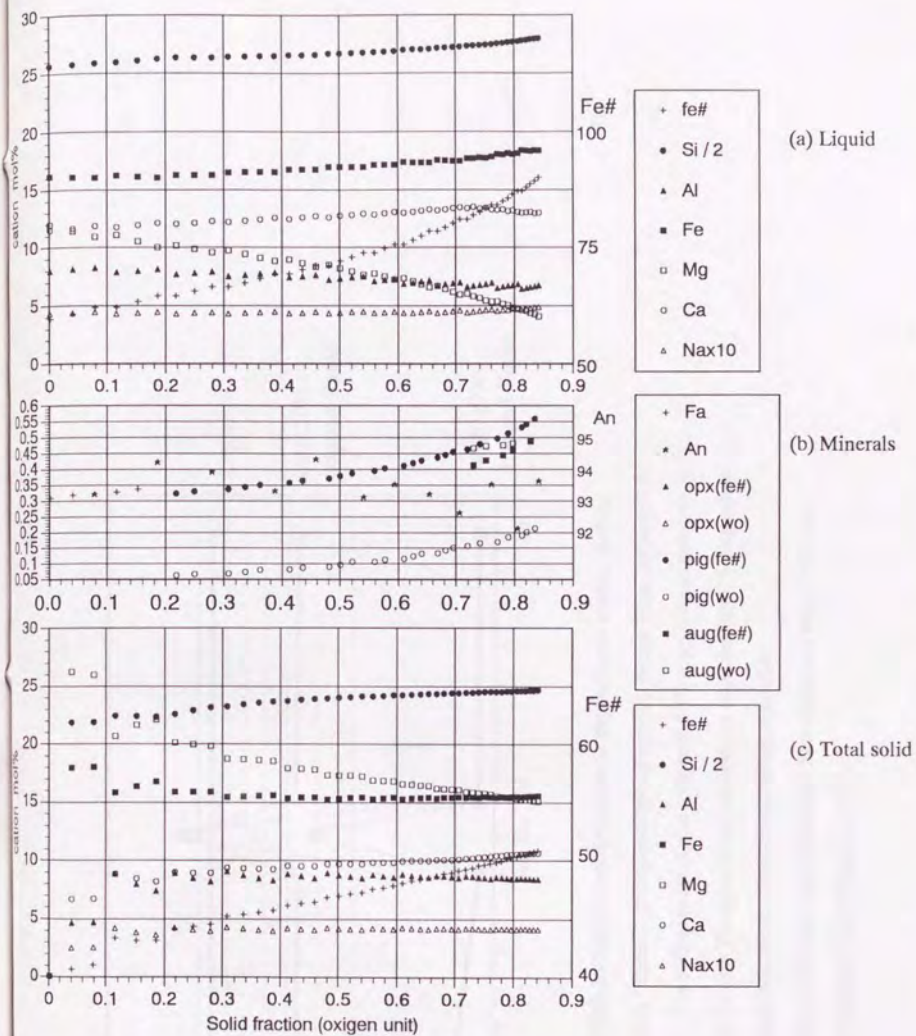


Fig.13 The results of fractional crystallization simulation. (a) Chemical compositions of liquid path, (b) Crystallizing phase, (c) Chemical compositions of total solid.

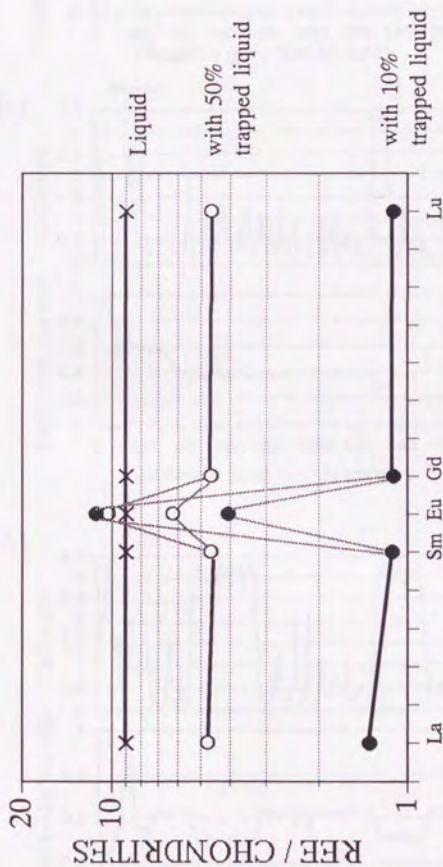


Fig.14 Model REE patterns of cumulate eucrite in trapped liquid model. Starting material is shown as "liquid". It is an analogue of ordinary eucrite (e.g. Juvinas) with REE by 9 x CCI. The REE patterns of total solid with 50% trapped liquid and with 10 % trapped liquid are shown. The crystallizing minerals are estimated 32vol.% plagioclase and 68 vol% olivine from the fractional crystallization simulation.

Sources of partition coefficients: plagioclase/melt from Drake and Weill (1975) and olivine/melt from Schnetzler and Philpotts (1970).

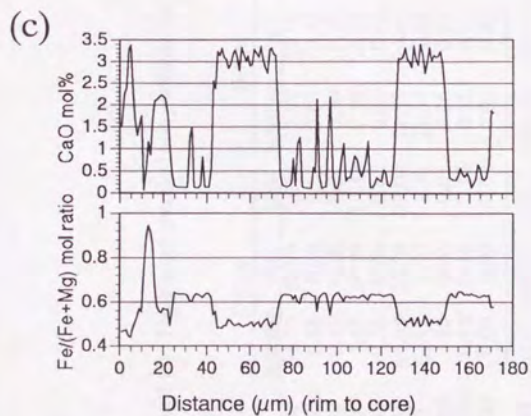
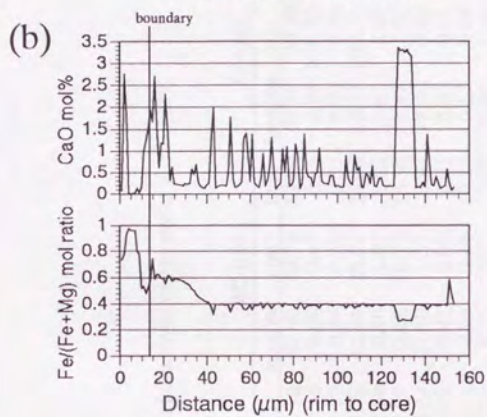
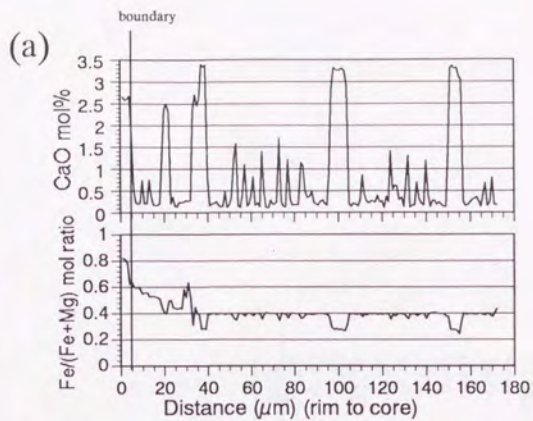


Fig.15 The chemical zoning and exsolution profile of pyroxene in Y82009 (a) (b), and the exsolution profile of pyroxene in Y791192 (c).

Table 1 (a) The average chemical compositions (wt. %) of four types of pyroxenes in Y791439.

	D-type		B-type		MC-type		JV-type	
	lamellae	host	lamellae	host	lamellae	host	lamellae	host
SiO ₂	53.77	53.74	52.97	52.10	51.90	50.74	50.82	50.71
Al ₂ O ₃	0.88	0.50	0.64	0.45	0.46	0.49	0.53	0.76
TiO ₂	0.47	0.20	0.39	0.29	0.29	0.31	0.32	0.50
FeO	7.65	19.79	9.58	24.55	23.70	28.02	26.88	18.75
MnO	0.36	0.66	0.34	0.82	0.80	1.07	1.02	0.61
MgO	15.08	23.28	23.04	20.40	20.07	16.59	16.30	9.47
CaO	22.12	1.72	21.64	1.08	2.24	1.52	2.97	18.30
Na ₂ O	0.10	0.01	0.06	0.01	0.01	0.01	0.01	0.05
Cr ₂ O ₃	0.46	0.16	0.15	0.11	0.11	0.26	0.16	0.17
V ₂ O ₃	0.09	0.02	0.05	0.02	0.01	0.02	0.02	0.00
Total	101.0	100.1	100.1	100.46	100.45	98.95	99.07	99.31
Ca*		4.68		4.60			6.37	
Mg		64.71		57.39			48.64	
Fe		30.61		38.01			44.99	
No. of analyses	3	21	4	30	3	6	1	11

* Atomic percent.

Table 1 (b) The average chemical compositions (wt.%) of four types of pyroxenes in Y791192.

	D1-type		D2-type		B-type		MCI-type	
	bulk	lamellae	bulk	host	lamellae	host	bulk	host
SiO ₂	-	53.61	53.19	52.55	53.04	52.47	52.54	51.45
Al ₂ O ₃	-	0.56	0.74	0.59	0.53	0.45	0.46	0.38
TiO ₂	-	0.21	0.37	0.26	0.39	0.26	0.27	0.20
FeO	-	19.99	10.40	223.41	9.34	24.36	22.48	28.08
MnO	-	0.69	0.48	0.79	0.35	0.84	0.78	0.93
MgO	-	23.52	15.01	21.24	20.97	14.15	19.38	17.35
CaO	-	1.13	20.62	1.25	2.05	22.39	3.53	21.61
Na ₂ O	-	0.00	0.07	0.01	0.05	0.00	0.01	0.05
Cr ₂ O ₃	-	0.29	0.38	0.278	0.31	0.16	0.18	0.13
V ₂ O ₃	-	0.02	0.05	0.02	0.02	0.01	0.01	0.02
Total	-	100.1	100.36	100.42	100.60	98.95	99.68	99.712
Ca*		2.28		4.16		7.20		14.33
Mg		66.17		59.47		56.18		47.17
Fe		31.54		36.36		36.61		38.50
No. of analyses		14	1	23	2	14	2	5

	MC2-type		JV-type	
	lamellae	host	lamellae	host
SiO ₂	52.23	51.22	51.42	49.95
Al ₂ O ₃	0.74	0.31	0.40	0.32
TiO ₂	0.43	0.20	0.25	0.16
FeO	11.88	29.77	26.19	34.86
MnO	0.39	1.01	0.89	1.11
MgO	12.72	16.39	15.66	10.62
CaO	21.38	0.72	4.85	21.00
Na ₂ O	0.07	0.01	0.02	0.09
Cr ₂ O ₃	0.32	0.10	0.14	0.24
V ₂ O ₃	0.03	0.02	0.03	0.04
Total	100.22	100.1	99.87	100.66
Ca*		10.07		15.10
Mg		46.34		35.20
Fe		43.59		49.70
No. of analyses	2	8	4	11

* Atomic percent.

Table 1 (c) The average chemical compositions (wt. %) of four types of pyroxenes in Y82009.

	D-type		B-type		MC-type		JV-type			
	lamellae	host	lamellae	host	lamellae	host	lamellae	host		
SiO ₂	-	53.93	52.85	52.47	52.50	-	51.21	49.23	49.73	49.68
Al ₂ O ₃	-	1.06	0.97	0.56	0.58	-	0.58	1.50	0.94	1.00
TiO ₂	-	0.16	0.58	0.32	0.34	-	0.56	1.27	0.27	0.37
FeO	-	17.78	10.30	23.25	22.41	-	26.16	18.70	32.15	30.81
MnO	-	0.66	0.51	0.80	0.78	-	0.81	0.64	0.97	0.94
MgO	-	23.92	14.79	20.73	20.35	-	16.31	10.39	12.96	12.71
CaO	-	2.32	19.75	1.53	2.71	-	4.24	17.48	2.83	4.30
Na ₂ O	-	0.02	0.09	0.01	0.02	-	0.04	0.06	0.02	0.02
Cr ₂ O ₃	-	0.74	0.41	0.35	0.35	-	0.32	0.52	0.27	0.29
V ₂ O ₃	-	0.04	0.04	0.02	0.02	-	0.02	0.08	0.04	0.05
Total	-	100.6	100.3	100.0	100.0	-	100.2	99.31	100.2	100.2
Ca*		4.68			5.59		8.95			9.30
Mg		67.2			58.3		47.9			38.3
Fe		28.1			36.0		43.1			52.31
No. of analyses	9	6	2	29			1	9		

	Z-type	
	lamellae	host
SiO ₂	-	49.62
Al ₂ O ₃	-	1.25
TiO ₂	-	0.49
FeO	-	25.51
MnO	-	0.85
MgO	-	10.72
CaO	-	10.43
Na ₂ O	-	0.037
Cr ₂ O ₃	-	0.16
V ₂ O ₃	-	0.02
Total	-	100.1
Ca*		23.5
Mg		32.3
Fe		44.2
No. of analyses		17

Table 1 (d) The average chemical compositions (wt. %) of four types of pyroxenes in Y82049.

	D1-type		D2-type		B-type		JV1-type	
	lamellae	host	lamellae	host	lamellae	host	lamellae	host
SiO ₂	-	-	54.18	-	52.18	51.94	51.98	51.55
Al ₂ O ₃	-	0.83	-	1.10	0.64	0.37	0.42	0.60
TiO ₂	-	0.11	-	0.16	0.33	0.21	0.23	0.53
FeO	-	15.55	-	20.47	12.10	25.82	23.29	14.33
MnO	-	0.55	-	0.77	0.52	0.93	0.85	0.52
MgO	-	26.98	-	20.97	13.31	18.88	17.85	11.97
CaO	-	1.24	-	2.95	20.64	1.61	5.12	20.27
Na ₂ O	-	0.01	-	0.02	0.05	0.01	0.02	0.07
Cr ₂ O ₃	-	0.77	-	0.70	0.30	0.22	0.23	0.50
V ₂ O ₃	-	0.02	-	0.02	0.06	0.01	0.02	0.02
Total	-	100.2	-	100.0	100.1	100.0	100.0	100.3
Ca*	-	2.44	-	6.12	-	-	10.55	-
Mg	-	73.70	-	60.67	-	-	51.63	-
Fe	-	23.85	-	33.20	-	-	37.81	-
No. of analyses	21		29		7	31	5	9

	JV2-type		JV3-type		Z-type	
	lamellae	host	lamellae	host	lamellae	host
SiO ₂	50.21	49.88	50.02	48.97	48.82	-
Al ₂ O ₃	0.44	0.35	0.39	1.25	0.55	-
TiO ₂	0.23	0.27	0.25	0.61	0.20	0.30
FeO	30.37	33.43	32.07	23.28	38.52	34.71
MnO	1.05	1.15	1.10	0.83	1.38	1.24
MgO	12.15	12.61	12.41	7.76	8.33	8.19
CaO	5.84	1.77	3.58	15.69	1.74	5.23
Na ₂ O	0.02	0.01	0.02	0.07	0.02	0.03
Cr ₂ O ₃	0.21	0.58	0.42	0.21	0.12	0.14
V ₂ O ₃	0.00	0.02	0.01	0.03	0.03	0.03
Total	100.5	100.1	100.3	98.72	99.43	99.25
Ca*	-	7.74	-	11.78	-	19.58
Mg	-	37.66	-	26.06	-	37.31
Fe	-	54.59	-	62.15	-	43.10
No. of analyses	4	5	1	3	7	7

Table 2. The average chemical compositions (wt%) of cumulate eucrites.

	Y791195		Medanitos		Nagaria		ALH85001	
	lamellae	host	lamellae	host	lamellae	host	lamellae	host
SiO ₂	51.40	49.98	53.25	52.73	51.91	50.29	53.04	53.27
Al ₂ O ₃	0.63	0.18	0.58	0.42	0.57	0.37	0.85	0.59
TiO ₂	0.39	0.18	0.06	0.05	0.35	0.89	0.45	0.28
FeO	16.01	31.71	9.16	23.78	11.37	28.36	9.58	21.20
MnO	0.54	1.08	0.40	0.82	0.44	0.92	0.41	0.75
MgO	11.32	13.40	15.14	20.45	13.05	17.24	16.08	22.68
CaO	18.64	2.41	20.25	0.96	21.56	1.09	19.02	1.19
Na ₂ O	0.06	0.01	0.05	0.01	0.05	0.01	0.06	0.00
Cr ₂ O ₃	0.25	0.11	0.54	0.18	0.24	0.16	0.31	0.19
V ₂ O ₃	0.01	0.02	0.05	0.02	0.03	0.03	0.02	0.02
Total	99.27	99.11	99.49	99.45	99.61	99.39	99.84	100.21
No. of analyses	9	30	5	29	15	56	17	99

Table 3. The average chemical compositions (wt%) of plagioclase in cumulate eucrites.

	Y791195	Medanitos	Nagaria	ALH85001
SiO ₂	45.34	45.10	44.74	45.29
Al ₂ O ₃	34.32	35.35	34.67	35.01
TiO ₂	0.01	0.01	0.02	0.03
FeO	0.14	0.12	0.11	0.13
MnO	0.02	0.02	0.02	0.02
MgO	0.02	0.02	0.02	0.07
CaO	18.23	18.94	18.38	17.72
Na ₂ O	0.98	0.64	0.93	0.23
K ₂ O	0.06	0.04	0.04	0.55
Cr ₂ O ₃	0.02	0.03	0.02	0.02
V ₂ O ₃	0.01	0.02	0.02	0.02
NiO	0.02	0.02	0.03	0.02
Total	99.19	100.29	99.00	99.11
Or*	0.34	0.25	0.26	3.58
Ab	8.84	5.74	8.34	2.12
An	90.82	94.02	91.40	94.30
An range	89 - 93	93 - 95	90 - 94	91 - 94
No. of analyses	62	28	16	51

* mol %

Table 4. Modal abundance (areal %) * of four types of pyroxenes in Y791439.

Pyroxene type phase	D-type		B-type		MC-type		JV-type	
	host	lamellae	host	lamellae	host	lamellae	host	lamellae
areal %	18.87	0.50	61.74	3.95	5.77	0.48	7.37	1.32
L/H ratios		0.026		0.064		0.083		0.18
No. of points	13590	360	44473	2847	4156	347	5306	951

*These data are normalized to 100% for the entire surface of pyroxene grains.

Appendix I

The procedures of computer simulations

In this study the author performed three kinds of computer simulations. Those are (Work A) Equilibrium liquid calculation. (The results are shown in Fig. 10 and Fig. 11)

(Work B) Mafic element fractionation with/without trapped liquid.

(The result is shown in Fig.12)

(Work C) Fractional crystallization with trapped liquid.

(The result is shown in Fig.13)

This section shows the procedures of simulation programs. All programs in this sections are written by "MS-C ver.6". But they can be compiled by other C language. The output of these programs are given by text file. The author make the result-figures (Fig.12 and 13) by arranging the text files with "DeltaGraph professional for macintosh".

In all work, the author applied the mineral/melt partition coefficients of Nielsen and Drake (1979) for pyroxene and those of Nielsen and Dungan (1983) for other minerals.

These partition coefficients are calculated from activities of elements. The activities are calculated by following equations.

l_NM : total mol of network forming element.
 l_NF : total mol of network modifying element.
 $lmo["element_name"]$: oxide mol % of element in silicate melt.
"element_name" $_NM$: activity of element in the network forming element.
"element_name" $_NF$: activity of element in the network modifying element.

$$l_NM = lmo[MG] + (lmo[AL] - lmo[NA] - lmo[K]) + lmo[CA] \\ + lmo[TI] + lmo[CR] + lmo[FE] + lmo[MN];$$
$$l_NF = lmo[SI] + lmo[NA] + lmo[K];$$
$$na_NF = lmo[NA] / l_NF;$$
$$mg_NM = lmo[MG] / l_NM;$$
$$al_NM = (lmo[AL] - lmo[NA] - lmo[K]) / l_NM;$$
$$al_NF = (lmo[NA] + lmo[K]) / l_NF;$$
$$si_NF = lmo[SI] / l_NF;$$
$$k_NF = lmo[K] / l_NF;$$
$$ca_NM = lmo[CA] / l_NM;$$
$$ti_NM = lmo[TI] / l_NM;$$
$$cr_NM = lmo[CR] / l_NM;$$
$$fe_NM = lmo[FE] / l_NM;$$
$$mn_NM = lmo[MN] / l_NM;$$

The activity of elements in minerals are calculated by following equations.

temp: equilibrium temperature (K)

Olivine

OL_mg: Mg₂SiO₄ activity in olivine

OL_fe: Fe₂SiO₄ activity in olivine

OL_mn: Mn₂SiO₄ activity in olivine

$$OL_mg = mg_NM * si_NF^{0.5} * \exp(6700 / temp - 3.73)$$

$$OL_fe = fe_NM * si_NF^{0.5} * \exp(6874 / temp - 4.97)$$

$$OL_mn = mn_NM * si_NF^{0.5} * \exp(9091 / temp - 6.7)$$

$$OL_total = OL_mg + OL_fe + OL_mn$$

Plagioclase

PL_ab: albite activity in plagioclase

PL_an: anorthite activity in plagioclase

$$PL_ab = 5 * na_NF * si_NF^3 * \exp(9031 / temp - 6.25)$$

$$PL_an = 5 * ca_NM * al_NM^2 * si_NF^2 * \exp(16667 / temp - 9.32)$$

Low-Ca pyroxene

LPX_mg: MgSiO₃ activity in pyroxene

LPX_fe: FeSiO₃ activity in pyroxene

LPX_ca: CaSiO₃ activity in pyroxene

LPX_al: Al₂O₃ activity in pyroxene

LPX_ti: TiO₂ activity in pyroxene

LPX_cr: Cr₂O₃ activity in pyroxene

$$LPX_mg = mg_NM * si_NF * \exp(5351 / temp - 2.553)$$

$$LPX_fe = fe_NM * si_NF * \exp(4488 / temp - 3.182)$$

$$LPX_ca = ca_NM * si_NF * \exp(28240 / temp - 20.684)$$

$$LPX_al = al_NM * \exp(30000 / temp - 23.7)$$

$$LPX_ti = ti_NM * \exp(6250 / temp - 6.25)$$

$$LPX_cr = cr_NM * \exp(10530 / temp - 6.3)$$

High-Ca pyroxene

HPX_mg: MgSiO₃ activity in pyroxene

HPX_fe: FeSiO₃ activity in pyroxene

HPX_ca: CaSiO₃ activity in pyroxene

HPX_al: Al₂O₃ activity in pyroxene

HPX_ti: TiO₂ activity in pyroxene

HPX_cr: Cr₂O₃ activity in pyroxene

$$HPX_mg = mg_NM * si_NF * \exp(6360 / temp - 3.59)$$

$$HPX_fe = fe_NM * si_NF * \exp(4709 / temp - 3.904)$$

$$HPX_ca = ca_NM * si_NF * \exp(4194 / temp - 2.53)$$

$$HPX_al = al_NM * \exp(23350 / temp - 18.54)$$

$$HPX_ti = ti_NM * \exp(4902 / temp - 5.43)$$

$$HPX_cr = cr_NM * \exp(36000 / temp - 24.7)$$

Work A

In the calculation of equilibrium liquid, the equations of low-Ca pyroxenes are applied.

Work B

For examining the efficiency of trapped liquid, the author made a simulation program for fractional crystallization of mafic minerals with/without trapped liquid. This simulation only handle Fe and Mg. This program prepares hypothetical liquid composed of FeO and MgO. Then it calculates IS composition using Fe/Mg partition coefficient of pyroxene and fractionate hypothetical pyroxene composed of MgO and FeO with 0.1 vol % of initial volume. This calculation is repeated until solid fraction reaches 95 vol %. For the calculation, partition coefficient between pyroxene and liquid ($K_p=0.29$) is applied.

The source list of this program is shown below.

[source list 1]

```
#include <stdio.h>
#include <math.h>

main()
{
    FILE    *fp,*fopen();
    double  fe_init,mg_init;
    double  l_fe,l_mg;           /* total liquid */
    double  s_fe,s_mg;         /* instantaneous solid */
    double  t_fe,t_mg;         /* instantaneous trapped liquid */
    double  liq_mg_fe;
    double  sol_mg_fe;
    double  f;
    double  liq_fe_number;
    double  sol_fe_number;
    double  k;
    double  step;
    double  ratio;

    k = 3.4; /* k = 1/KD */
    step = 100;
    fp=fopen("result.dat","w");

    printf("\nFe/(Fe+Mg) please!(0-1.0) ");
    scanf("%f",&liq_fe_number);
    printf("\nRatio of trapped liquid please!(0-1.0) ");
```


is originally written by MS-C ver.6 but other C-language can compile its source code.

The source code is listed as List.2.

2) The source code of MAGDIF is easy to read and reconstruct without the help of the author, because the structure of program has been completely rearranged for users preventing it to be a black box.

3) For the calculation of the chemical compositions of minerals in crystallization, MAGFOX and MAGDIF apply completely different ways. MAGFOX take much of temperature. When the chemical compositions calculated from partition coefficient are inconsistent with stoichiometry, MAGFOX put a priority on major elements and force to fit stoichiometry by ignoring equilibrium compositions of minor elements. MAGFOX take much of equilibrium compositions than temperature. It calculate equilibrium compositions and equilibrium temperature from liquid compositions. The calculated temperature often runs off the descendant line.

4) In fractionation process, MAGDIF can add trapped liquid to solid phase.

5) In fractionation, MAGFOX fractionates fixed mol of minerals but MAGDIF fractionates fixed amount of oxygen. 100 mol of liquid and 100 mol of olivine have different weight and volume. However 100 oxygen liquid and 100 oxygen olivine have similar volume. For the trapped liquid calculation, oxygen unit is more convenience.

In this simulation program chemical compositions of liquid are first converted to mol % oxides and then transformed into four major mineral components: Olivine (OL), Plagioclase (Pl), Wollastonite (Wo), and SiO₂ with TiO₂, Cr₂O₃, and trace elements being ignored. Of these quaternary coordinates, only Wo is employed in the parameterizations.

$$wo = (CaO - Al_2O_3 + K_2O + Na_2O) / (SiO_2 - Al_2O_3 - 3 * K_2O - 3 * Na_2O)$$

where the oxide symbols refer to mol %. A subprojection is then made from the Wo component onto the Ol[wo]-Pl[wo]-SiO₂[wo] plane, where [] indicates the component projected from

$$\begin{aligned} \text{Sum} &= \text{SiO}_2 - \text{CaO} - 4 * (\text{Na}_2\text{O} + \text{K}_2\text{O}) \\ \text{SiO}_2[\text{wo}] &= (\text{SiO}_2 - 0.5 * (\text{FeO} + \text{MgO} + \text{MnO}) - \text{Al}_2\text{O}_3 - \text{CaO} \\ &\quad - 5 * (\text{Na}_2\text{O} + \text{K}_2\text{O})) / \text{Sum} \\ \text{Ol}[\text{wo}] &= 0.5 * (\text{FeO} + \text{MgO} + \text{MnO}) / \text{Sum} \\ \text{Pl}[\text{wo}] &= 1 - \text{Ol}[\text{wo}] - \text{SiO}_2[\text{wo}] \end{aligned}$$

These molar projection coordinates are then employed in the parameterizations.

$$Fe' = 1 - Mg' = FeO / (FeO + MgO)$$

the normative alkali feldspar fraction in feldspar

$$AFP = 2 * (Na_2O + K_2O) / (Al_2O_3 + Na_2O + K_2O)$$

The Longhis' parameterizations of liquidus boundaries are as follows

olv: Ol[wo]
qtz: SiO₂[wo]
bfm: Fe'
afp: AFP

olivine - low Ca pyroxene

$$ol_lcapyx = (0.4 - 0.32 * bfm^{0.5}) * (olv - 0.128) + 0.4 \\ + 0.08 * afp + 0.25 * (1 - 1.67 * bfm) * wo - 0.08 * afp * olv \\ / (1 + 0.08 * afp);$$

olivine - augite

$$ol_aug = 0.54 * (1 - 0.5 * afp) * olv - 0.158 * (1 - 0.8 * bfm - 0.8 * afp) \\ * qtz + 0.145 + 0.12 * afp^2 - 0.2 * bfm;$$

opx - pigeonite

$$opx_pig = (.10 - .50 * afp) * olv - .161 * qtz + 0.1 * bfm \\ - 0.85 * bfm^2 + 0.25 * afp + 0.282;$$

olivine - plagioclase

$$ol_pl = -.528 * (1 - .6 * afp) * (1 + .55 * bfm) * qtz + .50 \\ + .29 * bfm - 0.35 * (1 + .18 * bfm) * afp - 0.05 * afp^2 \\ + 0.1 * (1 - 1.67 * bfm) * wo;$$

low Ca pyroxene - plagioclase

$$lcapyx_pl = -.68 * (1 + .45 * bfm) * (1 - .60 * afp) * qtz \\ + .565 + 0.29 * bfm - 0.35 * (1 + 0.18 * bfm) * afp - 0.05 * afp^2;$$

low Ca pyroxene - augite

$$lcapyx_aug = .945 * olv + 0.3628 * (1 + 0.9 * bfm) * qtz - 0.204 + 0.15 * afp - 0.35 * bfm;$$

quartz boundary

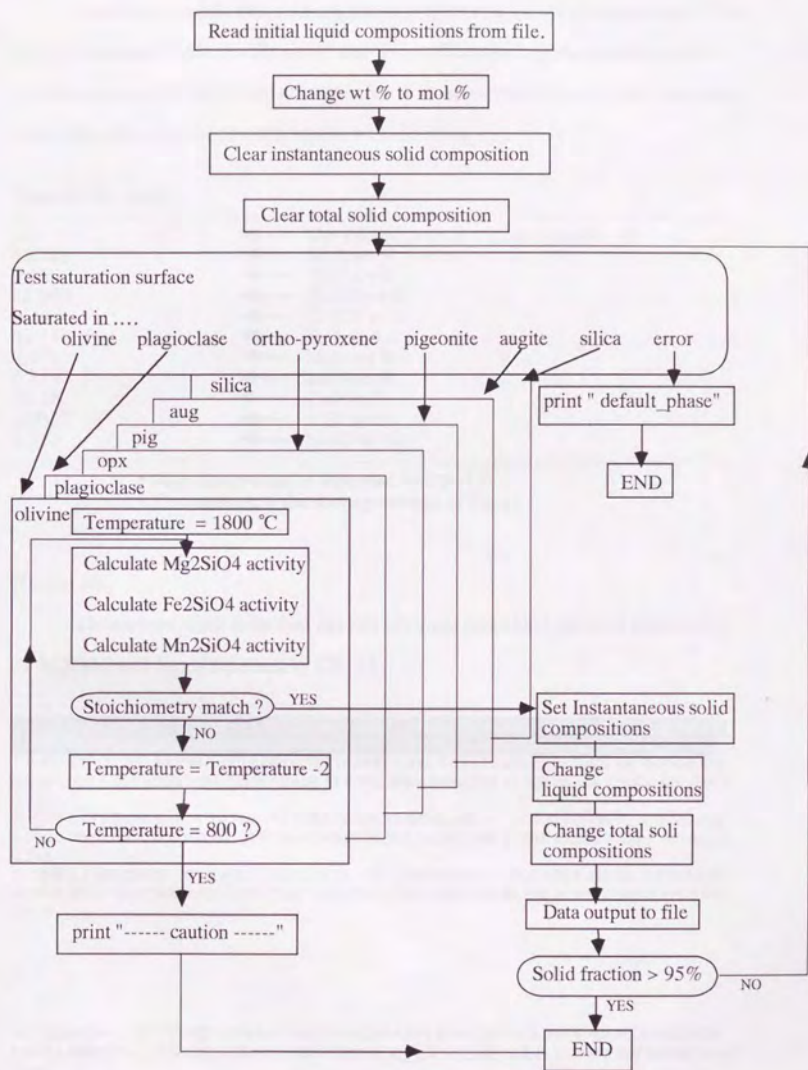
$$qtztes = -(0.2787 + 0.15 * (1 - bfm)) * (olv - 0.32 * bfm - .118) + 0.7 \\ - 0.33 * bfm + 0.333 * (1 - 0.5 * bfm) * wo + 0.533 * afp \\ - 0.533 * afp * olv / (1 + 0.533 * afp);$$

correction for high Ti liquid

```
ol_pl = ol_pl + (lmo[1]-4.0)*.009;  
ol_lcapyx = ol_lcapyx - (lmo[1]-4.0)*.0125;  
lcapyx_pl = lcapyx_pl + (lmo[1]-4.0)*.009;  
ol_aug = ol_aug - (lmo[1]-4.0)*.0125;  
lcapyx_aug = lcapyx_aug - (lmo[1]-4.0)*.0125;
```

Using Longhis' liquidus boundary equations and Nielsens' partition coefficient equations, MAGDIF calculates instantaneous crystallized mineral compositions and fractionate them with given ratio of trapped liquid. The procedures are shown at next flow diagram.





Flow chart of MAGDIF

Before you execute this program, please prepare data file of starting material. This program requests "input data file name" and "output file name" and then reads data file and makes output file on current directory. The formats of input data file which you make and output file which the program makes are as follows,

[Data file for input]

```

0.5          ← The volume ratio of trapped liquid (0 - 1)
49.248      ← SiO2 wt %
0.593       ← TiO2 wt %
12.969      ← Al2O3 wt %
0.36        ← Cr2O3 wt %
18.556      ← FeO wt %
7.678       ← MgO wt %
0.559       ← MnO wt %
10.25       ← CaO wt %
0.0367      ← K2O wt %
0.423       ← Na2O wt %
  
```

* Each datum must be separated by CR+LF
 * This example is the starting material of Fig.13

[Output file]

The inverted block is the first one line of output data. Each datum is separated by SPACE and each line is separated by CR+LF.

```

-----
0 1408 0.000 0.576 51.123 0.463 7.933 0.148 16.109 11.882 0.492 11.400 0.024 0.426 OL 0.307 0.000
0.000 0.000 0.000 0.000 0.000 0.000 * 0 0.000 0.000 0.000 0.000 0.000 0.000 0.000 0.000 0.000 0.000
1 1400 0.040 0.585 51.396 0.470 8.055 0.150 16.044 11.363 0.491 11.574 0.025 0.432 OL 0.316 0.000
0.000 0.000 0.000 0.000 0.000 0.000 * 0.406 43.607 0.268 4.598 0.086 17.896 26.169 0.508 6.607 0.014
0.247
2 1314 0.078 0.596 51.674 0.477 8.178 0.152 15.969 10.845 0.490 11.751 0.025 0.439 PL 0.000 0.932
0.000 0.000 0.000 0.000 0.000 0.000 * 0.410 43.670 0.270 4.629 0.086 17.993 25.925 0.512 6.651 0.014
0.248
3 1398 0.115 0.596 51.805 0.483 7.792 0.154 16.172 10.982 0.496 11.664 0.025 0.425 OL 0.326 0.000
0.000 0.000 0.000 0.000 0.000 0.000 * 0.433 44.809 0.278 8.780 0.089 15.765 20.619 0.455 8.776 0.015
0.414
.
.
.
.
45 1306 0.841 0.820 55.883 0.794 6.678 0.071 18.296 4.011 0.842 12.895 0.045 0.485 PL 0.000 0.936
0.000 0.000 0.000 0.000 0.000 0.000 * 0.508 49.213 0.357 8.315 0.162 15.509 15.024 0.397 10.596 0.018
0.408
46
Silica appears !
The End !
-----
  
```

The data are listed in the following order;

(1)Cycle, (2)Temperature, (3) solid_fraction, (4) fe' of liquid, (5)SiO₂ mol % of liquid, (6) TiO₂ mol % of liquid, (7) Al₂O₃ mol % of liquid, (8) Cr₂O₃ mol % of liquid, (9) Fe₂O₃ mol % of liquid, (10) MgO mol % of liquid, (11) MnO mol % of liquid, (12) CaO mol % of liquid, (13) K₂O mol % of liquid, (14) Na₂O mol % of liquid, Mineral_name (NON, OL, PL, OPX, PIG, AUG, SIL), (15) Fa content of olivine, (16) An content of plagioclase, (17) fe' of OPX, (18) wo of OPX, (19) fe' of PIG, (20) wo of PIG, (21) fe' of AUG, (22) wo of AUG, (23) "*" (separator)", (24) fe' of total solid, total solid (25) SiO₂ mol % of total solid, (26) TiO₂ mol % of total solid, (27) Al₂O₃ mol % of total solid, (28) Cr₂O₃ mol % of total solid, (29) Fe₂O₃ mol % of total solid, (30) MgO mol % of total solid, (31) MnO mol % of total solid, (32) CaO mol % of total solid, (33) K₂O mol % of total solid, and (34) Na₂O mol % of total solid, Si mol% of total solid.

The source code of MAGDIF follows.

[Source list 2 "MAGDIF.C"]

```
-----
#include <stdio.h>
#include <math.h>
#define POW(x,y) pow(x,(double)y)

#define NO_ELEMENT 10
#define SI 0
#define TI 1
#define AL 2
#define CR 3
#define FE 4
#define MG 5
#define MN 6
#define CA 7
#define K 8
#define NA 9

#define NO_PHASE 7
#define NON 0
#define OL 1
#define PL 2
#define OPX 3
#define PIG 4
#define AUG 5
#define SIL 6

#define NO_BOUND 7
#define OL_LCAPYX 0
#define OL_AUG 1
#define OPX_PIG 2
#define OL_PL 3
#define LCAPYX_PL 4
#define LCAPYX_AUG 5
#define QTZTES 6
```

```

FILE *fopen(),*fp1,*fp2;

double lw[NO_ELEMENT];
double lmo[NO_ELEMENT];

double isc[NO_ELEMENT];
double tsc[NO_ELEMENT];

double temp;
int phase;
double out_var[8];

double na_NF,mg_NM,al_NM,al_NF,si_NF,k_NF;
double ca_NM,ti_NM,cr_NM,fe_NM,mn_NM;

double liquid_o = 1;
double solid_o = 0;
double isc_o = 0;
double trapped; /* 0 - 1 */

void isc_clr()
{
    int n;
    for(n=0;n<NO_ELEMENT;n++) isc[n]=0;
}

void tsc_clr()
{
    int n;
    for(n=0;n<NO_ELEMENT;n++) tsc[n]=0;
}

void out_var_clr()
{
    int n;
    for(n=0;n<8;n++) out_var[n]=0;
}

void liquid()
{
    double l_NM,l_NF;

    l_NM = lmo[MG] + (lmo[AL] - lmo[NA] - lmo[K]) + lmo[CA]
           + lmo[TI] + lmo[CR] + lmo[FE] + lmo[MN];
    l_NF = lmo[SI] + lmo[NA] + lmo[K];

    na_NF = lmo[NA] / l_NF;
    mg_NM = lmo[MG] / l_NM;
    al_NM = (lmo[AL] - lmo[NA] - lmo[K]) / l_NM;
    al_NF = (lmo[NA] + lmo[K]) / l_NF;
    si_NF = lmo[SI] / l_NF;
    k_NF = lmo[K] / l_NF;
    ca_NM = lmo[CA] / l_NM;
    ti_NM = lmo[TI] / l_NM;
    cr_NM = lmo[CR] / l_NM;
    fe_NM = lmo[FE] / l_NM;
    mn_NM = lmo[MN] / l_NM;
}

```

```

/*-----*/
void data_input()
{
    unsigned char    filename1[13];
    unsigned char    filename2[13];

    printf("\nInput filename please ! \n");
    scanf("%s",filename1);

    printf("\nOutput filename please ! \n");
    scanf("%s",filename2);

    fp1 = fopen(filename1,"r");
    fp2 = fopen(filename2,"w");

    fscanf(fp1,"%lf",&trapped);
    fscanf(fp1,"%lf",&lw[S]);
    fscanf(fp1,"%lf",&lw[T]);
    fscanf(fp1,"%lf",&lw[AL]);
    fscanf(fp1,"%lf",&lw[CR]);
    fscanf(fp1,"%lf",&lw[FE]);
    fscanf(fp1,"%lf",&lw[MG]);
    fscanf(fp1,"%lf",&lw[MN]);
    fscanf(fp1,"%lf",&lw[CA]);
    fscanf(fp1,"%lf",&lw[K]);
    fscanf(fp1,"%lf",&lw[NA]);

}

void wt2mol()
{
    int n;
    double total = 0;
    int    mineral = 0;

    lmo[S] = lw[S]/60.084;
    lmo[T] = lw[T]/79.899;
    lmo[AL] = lw[AL]/101.96;
    lmo[CR] = lw[CR]/151.99;
    lmo[FE] = lw[FE]/71.846;
    lmo[MG] = lw[MG]/40.304;
    lmo[MN] = lw[MN]/70.937;
    lmo[CA] = lw[CA]/56.079;
    lmo[K] = lw[K]/39.098;
    lmo[NA] = lw[NA]/22.990;

    for(n=0;n<NO_ELEMENT;n++){
        total = total + lmo[n];
    }
    for(n=0;n<NO_ELEMENT;n++){
        lmo[n] = lmo[n]/total*100;
    }
}

```

```

int test_saturation()
{
    double bfm,sa,olv,qtz,wo,afp;
    double ol_lcapyx,ol_aug,opx_pig,ol_pl,lcapyx_pl,lcapyx_aug,qtztes;
    double pr = 0.0;
    int flag[NO_BOUND];
    int mineral = NON;

    int n;

    bfm=(lmo[FE]/(lmo[FE]+lmo[MG]));
    sa=(lmo[SI]-lmo[CA]-4.*lmo[K]-4.*lmo[NA]);
    olv=(lmo[FE]+lmo[MG]+lmo[MN])/2./sa;
    qtz=(lmo[SI]-0.5*(lmo[FE]+lmo[MG]+lmo[MN])-lmo[AL]-lmo[CA]
        -5.*(lmo[K]+lmo[NA]))/sa;
    wo=(lmo[CA]-lmo[AL]+lmo[K]+lmo[NA])/((lmo[SI]-lmo[AL]-3.*lmo[K]-3.*lmo[NA]));
    afp=2.*(lmo[NA]+lmo[K])/((lmo[AL]+lmo[K]+lmo[NA]));

    ol_lcapyx = (0.4-0.32*sqrt(bfm))*(olv-0.128)+0.4
        +0.08*afp+0.25*(1-1.67*bfm)*wo-0.08*afp*olv
        /(1+0.08*afp);

    ol_aug = 0.54*(1.-0.5*afp)*olv-0.158*(1.-0.8*bfm-0.8*afp)
        *qtz+0.145+0.12*pow(afp,2)-0.2*bfm;

    opx_pig = (.10-.50*afp)*olv-.161*qtz+0.1*bfm
        -0.85*pow(bfm,2)+0.25*afp+0.282;

    ol_pl = -.528*(1.-.6*afp)*(1.+.55*bfm)*qtz+.50
        +.29*bfm-0.35*(1.+.18*bfm)*afp-0.05*pow(afp,2)
        +0.1*(1-1.67*bfm)*wo;

    lcapyx_pl = -.68*(1.+.45*bfm)*(1.-.60*afp)*qtz
        +.565+0.29*bfm-0.35*(1+0.18*bfm)*afp-0.05*pow(afp,2);

    lcapyx_aug = .945*olv+0.3628*(1+0.9*bfm)*qtz-0.204+0.15*afp-0.35*bfm;

    if(lmo[1]>4.0){
        ol_pl = ol_pl + (lmo[1]-4.0)*.009;
        ol_lcapyx = ol_lcapyx - (lmo[1]-4.0)*.0125;
        lcapyx_pl = lcapyx_pl + (lmo[1]-4.0)*.009;
        ol_aug = ol_aug - (lmo[1]-4.0)*.0125;
        lcapyx_aug = lcapyx_aug - (lmo[1]-4.0)*.0125;
    }

    if(lcapyx_pl < 0.1) lcapyx_pl = 0.1;

    qtztes = -(0.2787+0.15*(1-bfm))*(olv-0.32*bfm-.118)+0.7
        -0.33*bfm+0.333*(1-0.5*bfm)*wo+0.533*afp
        -0.533*afp*olv/(1+0.533*afp);

    for(n=0;n<NO_BOUND;n++) flag[n]=0;

    if(qtz < ol_lcapyx) flag[OL_LCAPYX] = 1;
    if(wo < ol_aug) flag[OL_AUG] = 1;
    if(wo < opx_pig) flag[OPX_PIG] = 1;
    if(olv < ol_pl) flag[OL_PL] = 1;
    if(olv < lcapyx_pl) flag[LCAPYX_PL] = 1;
    if(wo < lcapyx_aug) flag[LCAPYX_AUG] = 1;
    if(qtz < qtztes) flag[QTZTES] = 1;

```

```

if((flag[OL_LCAPYX] == 1)&&
(flag[OL_AUG] == 1)&&
(flag[OL_PL] == 0)){
    mineral = OL;
    goto test_end;
}
if((flag[OL_LCAPYX] == 0)&&
(flag[LCAPYX_PL] == 0)&&
(flag[LCAPYX_AUG] == 1)){
    if(flag[OPX_PIG] == 1) mineral = OPX;
    else mineral = PIG;
}
if((flag[OL_AUG] == 0)&&
(flag[LCAPYX_AUG] == 0))
    mineral = AUG;

if((flag[OL_PL] == 1)&&
(flag[LCAPYX_PL] == 1))
    mineral = PL;

if(flag[QTZTES] == 0) mineral = SIL;

test_end:
    return(mineral);
}
/*-----*/

int olivine()
{
    double OL_mg,OL_fe,OL_mn,OL_total;
    double old_total = 0;
    double mag;

    for(temp = 1800; temp >800; temp=temp-2){
        OL_mg = mg_NM * POW(si_NF,.5) * exp(6700 / temp - 3.73);
        OL_fe = fe_NM * POW(si_NF,.5) * exp(6874 / temp - 4.97);
        OL_mn = mn_NM * POW(si_NF,.5) * exp(9091 / temp - 6.7);
        OL_total = OL_mg + OL_fe + OL_mn;
        OL_total = 1 - OL_total;
        if(OL_total * old_total < 0) break;
        old_total = OL_total;
    }

    if(temp != 800){
        isc_clr();
        out_var_clr();
        mag = isc_o /4;
        isc[Sil] = 1*mag;
        isc[MG] = OL_mg *2*mag;
        isc[FE] = OL_fe *2*mag;
        isc[MN] = OL_mn *2*mag;

        out_var[0] = OL_fe / (OL_mg + OL_fe);

        return(1);
    }
    else return(10);
}

```

```

/*-----*/
int plagioclase()
{
    double PL_ab, PL_an, PL_total;
    double old_total = 0;
    double mag;

    for(temp=1800; temp>800; temp=temp-2){
        PL_ab = 5 * na_NF * POW(si_NF,3)
            * exp(9031 / temp - 6.25);
        PL_an = 5 * ca_NM * POW(al_NM,2)
            * POW(si_NF,2) * exp(16667 / temp - 9.32);
        PL_total = PL_ab + PL_an;
        PL_total = 1 - PL_total;
        if(PL_total * old_total < 0) break;
        old_total = PL_total;
    }

    if(temp != 800){
        isc_clr();
        out_var_clr();

        mag = isc_o / 8;
        isc[S] = (2+PL_ab) * mag;
        isc[CA] = (PL_an) * mag;
        isc[AL] = (1+PL_an) * mag;
        isc[NA] = (PL_ab) * mag;

        out_var[1]=PL_an;
        return(1);
    }
    else return(10);
}
/*-----*/
int orthopyx()
{
    double LPX_mg, LPX_fe, LPX_ca, LPX_al, LPX_ti, LPX_cr, LPX_total;
    double old_total = 0;
    double mag;

    for(temp = 1800; temp>800; temp=temp-2){
        LPX_mg = mg_NM * si_NF * exp(5351 / temp - 2.553);
        LPX_fe = fe_NM * si_NF * exp(4488 / temp - 3.182);
        LPX_ca = ca_NM * si_NF * exp(28240 / temp - 20.684);
        LPX_al = al_NM * exp(30000 / temp - 23.7);
        LPX_ti = ti_NM * exp(6250 / temp - 6.25);
        LPX_cr = cr_NM * exp(10530 / temp - 6.3);
        LPX_total = LPX_mg + LPX_fe + LPX_ca;
        LPX_total = 1 - LPX_total;
        if(LPX_total * old_total < 0) break;
        old_total = LPX_total;
    }
}

```

```

if(temp != 800){
    isc_clr();
    out_var_clr();
    mag = isc_o /3;
    isc[S] = 1 * mag;
    isc[MG] = LPX_mg * mag;
    isc[FE] = LPX_fe * mag;
    isc[CA] = LPX_ca * mag;
    isc[AL] = LPX_al * mag;
    isc[TI] = LPX_ti * mag;
    isc[CR] = LPX_cr * mag;

    out_var[2]=LPX_fe / (LPX_mg + LPX_fe);
    out_var[3]=LPX_ca;
    return(1);
}

else return(10);

}

/*-----*/
int pigeonite()
{
    double LPX_mg,LPX_fe,LPX_ca,LPX_al,LPX_ti,LPX_cr,LPX_total;
    double old_total = 0;
    double mag;

    for(temp = 1800; temp>800; temp=temp-2){
        LPX_mg = mg_NM * si_NF * exp(5351 / temp - 2.553);
        LPX_fe = fe_NM * si_NF * exp(4488 / temp - 3.182);
        LPX_ca = ca_NM * si_NF * exp(28240 / temp - 20.684);
        LPX_al = al_NM * exp(30000 / temp - 23.7);
        LPX_ti = ti_NM * exp(6250 / temp - 6.25);
        LPX_cr = cr_NM * exp(10530 / temp - 6.3);
        LPX_total = LPX_mg + LPX_fe + LPX_ca;
        LPX_total = 1 - LPX_total;
        if((LPX_total * old_total < 0) break;
        old_total = LPX_total;
    }
    if(temp != 800){
        isc_clr();
        out_var_clr();

        mag = isc_o /3;
        isc[S] = 1 * mag;
        isc[MG] = LPX_mg * mag;
        isc[FE] = LPX_fe * mag;
        isc[CA] = LPX_ca * mag;
        isc[AL] = LPX_al * mag;
        isc[TI] = LPX_ti * mag;
        isc[CR] = LPX_cr * mag;

        out_var[4]=LPX_fe / (LPX_mg + LPX_fe);
        out_var[5]=LPX_ca;
        return(1);
    }

    else return(10);

}

```

```

/*-----*/
int augite()
{
    double HPX_mg,HPX_fe,HPX_ca,HPX_al,HPX_ti,HPX_cr,HPX_total;
    double old_total = 0;
    double mag;

    for(temp = 1800; temp>800; temp=temp-2){
        HPX_mg = mg_NM * si_NF * exp(6360 / temp - 3.59);
        HPX_fe = fe_NM * si_NF * exp(4709 / temp - 3.904);
        HPX_ca = ca_NM * si_NF * exp(4194 / temp - 2.53);
        HPX_al = al_NM * exp(23350 / temp - 18.54);
        HPX_ti = ti_NM * exp(4902 / temp - 5.43);
        HPX_cr = cr_NM * exp(36000 / temp - 24.7);
        HPX_total = HPX_mg + HPX_fe + HPX_ca;
        HPX_total = 1 - HPX_total;
        if((HPX_total * old_total < 0) break;
        old_total = HPX_total;
    }

    if(temp != 800){
        isc_clr();
        out_var_clr();
        mag = isc_o / 3;
        isc[S] = 1 * mag;
        isc[MG] = HPX_mg * mag;
        isc[FE] = HPX_fe * mag;
        isc[CA] = HPX_ca * mag;
        isc[AL] = HPX_al * mag;
        isc[TI] = HPX_ti * mag;
        isc[CR] = HPX_cr * mag;

        out_var[6] = HPX_fe / (HPX_mg + HPX_fe);
        out_var[7] = HPX_ca;
        return(1);
    }
    else return(10);
}
/*-----*/
int silica()
{
    fprintf(fp2, "\n Silica appears ! ");
    return(1);
}

```

```

/*-----*/
void output()
{
    int n;
    fprintf(fp2, "%5.0f %5.3f", temp, solid_o);
    fprintf(fp2, "%5.3f", lmo[FE]) / (lmo[FE] + lmo[MG]);
    for(n=0; n<NO_ELEMENT; n++)
        fprintf(fp2, "%5.3f", lmo[n]);
    switch(phase){
        case NON:    fprintf(fp2, "NON");
                    break;
        case OL:     fprintf(fp2, "OL ");
                    break;
        case PL:     fprintf(fp2, "PL ");
                    break;
        case OPX:    fprintf(fp2, "OPX");
                    break;
        case PIG:    fprintf(fp2, "PIG");
                    break;
        case AUG:    fprintf(fp2, "AUG");
                    break;
        case SIL:    fprintf(fp2, "SIL");
                    break;
    }
    for(n=0; n<8; n++)
        fprintf(fp2, "%5.3f", out_var[n]);
    if(tsc[FE]==0) fprintf(fp2, " * 0");
    else fprintf(fp2, " * %5.3f", tsc[FE] / (tsc[FE] + tsc[MG]));
    for(n=0; n<NO_ELEMENT; n++)
        fprintf(fp2, "%5.3f", tsc[n]);
}

```

```

/*-----*/
void fractionation()
{
    int n;
    double total;

    total = 0;
    for(n=0; n<NO_ELEMENT; n++){
        lmo[n] = lmo[n] / 100 * liquid_o - isc[n];
        total = total + lmo[n];
    }
    for(n=0; n<NO_ELEMENT; n++){
        lmo[n] = lmo[n] / total * 100;
        if(lmo[n] < 0.01) lmo[n] = 0.01;
    }

    total = 0;
    for(n=0; n<NO_ELEMENT; n++){
        tsc[n] = tsc[n] / 100 * solid_o + isc[n]
                + lmo[n] / 100 * isc_o * trapped*2;
        total = total + tsc[n];
    }
    if(total != 0)
        for(n=0; n<NO_ELEMENT; n++){
            tsc[n] = tsc[n] / total * 100;
        }
    solid_o = solid_o - isc_o * (1 + trapped*2);
    liquid_o = liquid_o - isc_o * (1 + trapped*2);
}

```

```

/*-----*/
main()
{
    int    count;
    int    check;

    int    l,m,n;

    data_input();
    wt2mol();
    isc_clr();
    tsc_clr();

    for(count=0;count<1000;count++){
        isc_o = liquid_o * 0.02;
        phase = test_saturation();
        liquid();
        fprintf(fp2,"%n%d ",count);
        switch(phase){
            case OL:      check = olivine();
                          break;
            case PL:      check = plagioclase();
                          break;
            case OPX:     check = orthopyx();
                          break;
            case PIG:     check = pigeonite();
                          break;
            case AUG:     check = augite();
                          break;
            case SIL:     check = silica();
                          goto end;
            default:      fprintf(fp2,"%n default_phase");
                          goto end;
        }
        if(check > 9){
            fprintf(fp2,"\n-----caution-----\n");
            goto end;
        }
        output();
        fractionation();
        if(solid_o > 0.95){
            fprintf(fp2,"%n Liquid was used up!");
            goto end;
        }
    }
    end:  fprintf(fp2,"%n The End !\n");
         printf("\n The End !\n");
         fcloseall();
}

```

Appendix II

New utilization of Differential Thermal Analyses (DTA)

The author proposes a new utilization of DTA. That is the utilization for dynamic crystallization experiments. In this study the problem whether the degree of over saturation

affect the liquid path or not in the magma differentiation was tested.

Starting material

For the starting material, Fe-free magma analogs have been prepared, because our DTA has no gas control system. They were prepared from mixtures of oxides (Al_2O_3 , MgO , SiO_2 and CaCO_3). After weighing and mixing them in an alumina mortar for 24 hours, the reagents were heated at 1500°C for 2 hours in an 1 atm in the air. Then run-products were quenched into water. The quenched products are cracked and remixed in agate mortar for 15 minutes and reheated at 1500°C for 2 hours. After the reheating, run-products were quenched into water again. They are the final products for DTA experiments. The chemical compositions of starting materials are the mixture of forsterite 55 wt%, anorthite 25 wt% and SiO_2 20 wt%. According to the An-Fo- SiO_2 phase diagram, the first phase that crystallizes from this starting material is olivine, the second is pyroxene and the last is anorthite.

Methods

The DTA analysis were performed by TG-DTA 2000 (Mac Science Co.). The samples is heated at 1500°C for 2 hours and cooled to 1200°C in variable cooling rate. For all runs, the same sample, 10 mg in weight, has been used repeatedly. There is a possibility that the relict of crystal structure in the glass of previous run affects the results of next run. But the author took much of preventing the compositional change of starting material.

Results

The temperatures of peaks are slightly move in changing cooling late, because mainly of heat capacities of sample holder. The obtained peaks were roughly classified as peak 1, peak2, peak3 and peak4. The peak heights are characterized as follows, A: remarkable peak, B: clear peak, C: weak peak, x: no peak, and ?: hidden in noise. The results are shown in a table following. All peaks are exothermic peak.

Run No.	Cooling rate (°C/min)	peak 1 ~1230°C	peak 2 ~1320°C	peak 3 ~1350°C	peak 4 ~1420°C
1	0.5	x	x	x	x
2	0.5	C	x	x	C
3	0.5	x	x	C	x
4	5.0	?	?	C	?
5	8.0	A	x	B	A
6	10.0	B	A	x	B
7	10.0	A	x	x	B
8	10.0	A	B	x	A
9	10.0	A	C	C	A
10	12.0	A	C	C	A
11	15.0	x	x	x	B

The possible origins of peaks are, Peak A: crystallization of olivine, Peak B: crystallization of pyroxene, Peak C: crystallization of pyroxene and Peak D: crystallization of plagioclase. Peak2 and Peak3 may originally be one peak. In rapid cooling the system may split to two and two kinds of pyroxenes with different chemical compositions may be produced.

Discussion

The occurrence of peaks are different in changing cooling rate. For example, the results of 10°C/min (No.6 and 8) have three exothermic peaks but the result of 15°C/min has only one peak. These results can be interpreted as follows. In 10°C/min cooling rate, olivine crystallizes at first peak, then olivine reacts to pyroxene at second peak and plagioclase crystallizes at third peak. In 15°C/min cooling rate, olivine crystallized at first peak but there is no time to react to pyroxene. The No.1 result shows no peak. It is interpreted that there was no super saturation detected by DTA. The liquid drops on the

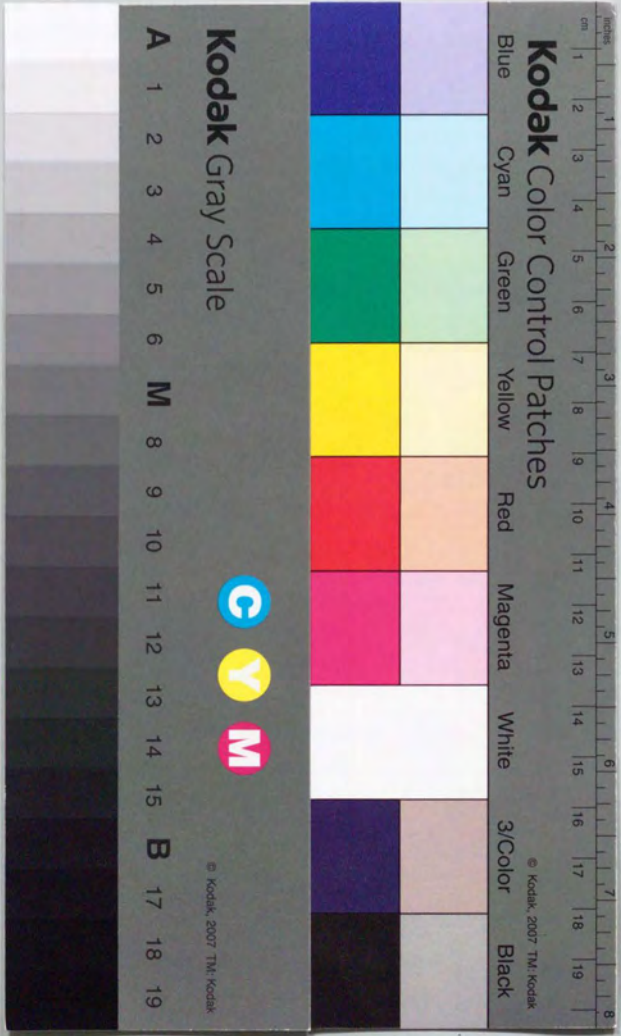
liquidus surface not peak but slope appears. The appearance of peak is indicate that the liquid drops on the solidus or be in super saturation. In the later case, it can be said that the height of the peak indicates the degree of super saturation and/or nucleation.

The remarkable point is that the run of the same starting material and the same cooling rate shows different results (No.6,7, and 8). These results suggest that the peak height of first phase affects that of second and later phase.

Using furnace, we could not know the relation ship between each crystallization stage, because once the sample has been quenched, we could not trace the further liquid path. The utilization of DTA would give us new information about dynamic crystallization.

For explaining the interval of chemical compositions of pyroxene in polymict eucrites, the author used to be applied the model that the liquid repeats oversaturation and crystallization. The results suggested that over saturation is not remarkable in slow cooling. The chemical compositions of this study is different from natural system. However, the physical process such as separation of system by convection layering are most likely to occur in HED parent body. The author supposed that olivine reaction would be a trigger for crystallization because the reaction cool the system. But in this work, there is no endothermic peak of olivine reaction observed.

卒論製本
ヤマザキ
22 (03) 3958-1681



Kodak Color Control Patches

Blue Cyan Green Yellow Red Magenta White 3/Color Black

Kodak Gray Scale

A 1 2 3 4 5 6 M 8 9 10 11 12 13 14 15 B 17 18 19



© Kodak, 2007 TM, Kodak